

A Bayesian approach to atmospheric circulation regime assignment

Article

Accepted Version

Falkena, S. K. J., de Wiljes, J., Weisheimer, A. and Shepherd, T. G. (2023) A Bayesian approach to atmospheric circulation regime assignment. *Journal of Climate*, 36. pp. 8619-8636. ISSN 1520-0442 doi: <https://doi.org/10.1175/JCLI-D-22-0419.1> Available at <https://centaur.reading.ac.uk/110936/>

It is advisable to refer to the publisher's version if you intend to cite from the work. See [Guidance on citing](#).

To link to this article DOI: <http://dx.doi.org/10.1175/JCLI-D-22-0419.1>

Publisher: American Meteorological Society

All outputs in CentAUR are protected by Intellectual Property Rights law, including copyright law. Copyright and IPR is retained by the creators or other copyright holders. Terms and conditions for use of this material are defined in the [End User Agreement](#).

www.reading.ac.uk/centaur

CentAUR

Central Archive at the University of Reading

Reading's research outputs online

A Bayesian Approach to Atmospheric Circulation Regime Assignment

Swinda K.J. Falkena,^a Jana de Wiljes,^{a,b} Antje Weisheimer,^{c,d} and Theodore G. Shepherd,^e

^a *Department of Mathematics and Statistics, University of Reading, Reading, UK*

^b *Institute for Mathematics, University of Potsdam, Potsdam, Germany*

^c *European Centre for Medium-Range Weather Forecasts (ECMWF), Reading, UK*

^d *National Centre for Atmospheric Science (NCAS), University of Oxford, Department of Physics,
Atmospheric, Oceanic and Planetary Physics (AOPP), Oxford, UK* ^e *Department of Meteorology,*

University of Reading, Reading, UK

⁹ *Corresponding author: Swinda K.J. Falkena, s.k.j.falkena@uu.nl*

10 ABSTRACT: The standard approach when studying atmospheric circulation regimes and their
11 dynamics is to use a hard regime assignment, where each atmospheric state is assigned to the
12 regime it is closest to in distance. However, this may not always be the most appropriate approach
13 as the regime assignment may be affected by small deviations in the distance to the regimes due
14 to noise. To mitigate this we develop a sequential probabilistic regime assignment using Bayes
15 Theorem, which can be applied to previously defined regimes and implemented in real time as new
16 data become available. Bayes Theorem tells us that the probability of being in a regime given the
17 data can be determined by combining climatological likelihood with prior information. The regime
18 probabilities at time t can be used to inform the prior probabilities at time $t + 1$, which are then used
19 to sequentially update the regime probabilities. We apply this approach to both reanalysis data
20 and a seasonal hindcast ensemble incorporating knowledge of the transition probabilities between
21 regimes. Furthermore, making use of the signal present within the ensemble to better inform
22 the prior probabilities allows for identifying more pronounced interannual variability. The signal
23 within the interannual variability of wintertime North Atlantic circulation regimes is assessed using
24 both a categorical and regression approach, with the strongest signals found during very strong El
25 Niño years.

26 SIGNIFICANCE STATEMENT: Atmospheric circulation regimes are recurrent and persistent
27 patterns that characterize the atmospheric circulation on timescales of one to three weeks. They
28 are relevant for predictability on these timescales as mediators of weather. In this study we propose
29 a novel approach to assigning atmospheric states to six pre-defined wintertime circulation regimes
30 over the North Atlantic and Europe, which can be applied in real time. This approach introduces a
31 probabilistic, instead of deterministic, regime assignment and uses prior knowledge on the regime
32 dynamics. It allows to better identify the regime persistence and indicates when a state does not
33 clearly belong to one regime. Making use of an ensemble of model simulations, we can identify
34 more pronounced interannual variability by using the full ensemble to inform prior knowledge on
35 the regimes.

36 **1. Introduction**

37 A thorough understanding of extra-tropical circulation variability on sub-seasonal timescales
38 is important for improving predictability on these timescales. Improvement of this predictability
39 is of great societal relevance for sectors such as renewable energy. Atmospheric circulation, or
40 weather, regimes can describe this variability by dividing the circulation into a small number
41 of states or patterns (Hannachi et al. 2017). These regimes are recurrent patterns that represent
42 the low-frequency variability in the atmospheric circulation. They have been studied for a long
43 time, starting with papers focusing on their identification (e.g Mo and Ghil 1988; Molteni et al.
44 1990; Vautard 1990; Michelangeli et al. 1995), with later research discussing their links with other
45 processes and surface impacts (e.g. Straus and Molteni 2004; Cassou et al. 2005; Charlton-Perez
46 et al. 2018; van der Wiel et al. 2019).

47 The most commonly used technique for identifying circulation regimes is k -means clustering
48 (e.g. Michelangeli et al. 1995; Straus et al. 2007; Matsueda and Palmer 2018). This method
49 separates the phase space into k clusters, where the data within each cluster are similar, but
50 dissimilar between the different clusters. The number of clusters k has to be set a priori, for which
51 several approaches such as a classifiability index (Michelangeli et al. 1995) or information criteria
52 (O’Kane et al. 2013) are used. One of the drawbacks of this clustering approach is that it yields a
53 hard, deterministic, assignment of the data to each of the regimes. This means that it is difficult to

54 quantify the uncertainty of the regime assignment, as data close to the regime centre is treated the
55 same as data that is only just (by distance) assigned to that regime.

56 The hard regime assignment of k -means clustering means that the result is susceptible to noise.
57 Consider Figure 1(a) which shows the distance of the data to two regimes in time for a real case
58 (discussed later in detail), over a period of 12 days. Initially, the data clearly is categorised to
59 belong to regime A, being significantly closer in distance to regime A than to regime B. However,
60 from day 7 to 9 the data makes a brief excursion into a part of the phase diagram that is closer to
61 regime B, after which it moves back to being closest to regime A. The question is whether this is
62 a real signal or simply the effect of noise. Since the regime dynamics is quite persistent in time it
63 is likely to be the latter, but this possibility is not picked up by the hard assignment of a standard
64 k -means clustering approach. Often a low-pass filter is applied to remove this high-frequency
65 variability (e.g. Straus et al. 2007; Grams et al. 2017), but in Falkena et al. (2020) it was shown
66 that low-pass filtering can lead to a bias in the observed regime frequencies.

67 Another solution is to use a regularised clustering algorithm which constrains, or bounds, the
68 number of transitions between the regimes so that it is in line with the natural metastability of the
69 underlying dynamics. Such an approach, first introduced in the context of clustering methods by
70 Horenko (2010), has for example been applied to discrete jump processes (Horenko 2011a) with
71 applications in computational sociology (Horenko 2011b) and for efficient classification in the
72 context of sparse data settings (Vecchi et al. 2022). In the context of atmospheric dynamics, time
73 regularisation has been used to study the Southern Hemispheric circulation (O’Kane et al. 2013),
74 the dynamics of the North Atlantic Oscillation (Quinn et al. 2021), and how to identify persistent
75 circulation regimes (Falkena et al. 2020). A regularised clustering method allows to better identify
76 the signal within the noise, but does require selecting a constraint parameter. This introduces a
77 parameter selection, where e.g. an information criterion is used to decide on a suitable constraint
78 value.

79 An alternative approach is to make the regime assignment probabilistic rather than deterministic,
80 allowing for a more nuanced and informative regime assignment in the presence of noise. Methods
81 such as mixture modelling provide such a probabilistic regime assignment (e.g. Hannachi and
82 O’Neill 2001; Smyth et al. 1999; Baldo and Locatelli 2022), but are not widely used. Hidden
83 Markov Models (HMMs) extend the mixture modelling approach by also taking into account the

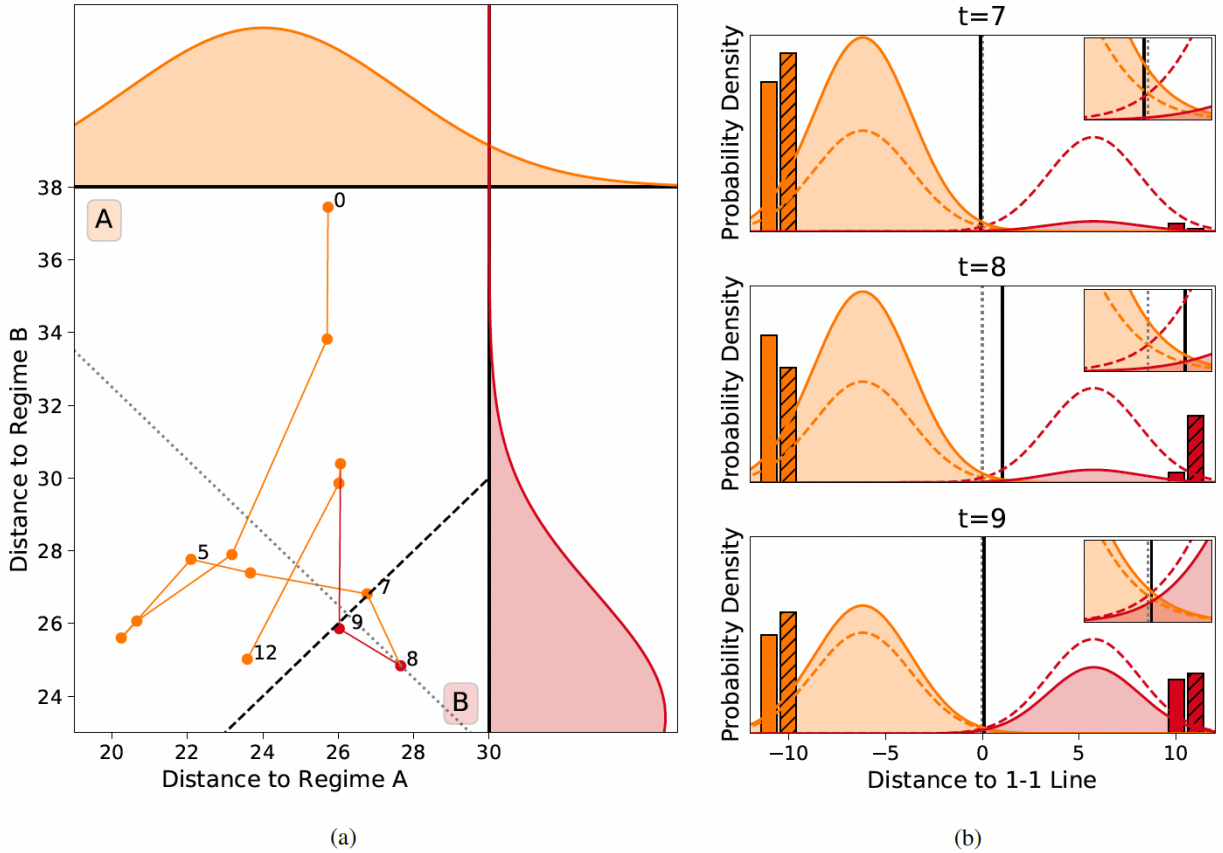


FIG. 1: A conceptual example of the difficulty k -means clustering has when noise affects the data, showing what a probabilistic approach can bring. (a) An example trajectory of the data as a function of the distances to two regimes A (orange) and B (red). The 1-1 line is shown black dashed, meaning the region above is closer to regime A and the region below to regime B. Numbers indicate the day corresponding to that point in the trajectory. The likelihood functions shown along the top and right give the climatological probability of those distances given hard assignment to regime A (orange, top) or B (red, right). The dotted grey line indicates a slice through the probability space along which the pdfs in panel (b) are considered. (b) A slice of the likelihood functions, weighted by the prior probabilities following Bayes Theorem, for each of the regimes (solid lines, A: orange, B: red) along the grey dotted line in (a), perpendicular to the 1-1 line, for the 7th, 8th, and 9th day. The location of the data on each day is indicated by the vertical black lines, and the bars at the edge of the plots show the prior (left) and posterior (right, hatched) probabilities for each of the regimes (A: orange, left edge, B: red, right edge). The climatological likelihood functions are shown dashed in all panels and the vertical grey dotted line indicates the location of the 1-1 line. The insets in each panel show an enlargement of the region around the 1-1 line.

84 dynamics of the system and not just the statistics (Majda et al. 2006; Franzke et al. 2008), but are
 85 hard to fit for relatively short timeseries when the data is high dimensional. Another approach
 86 is to approximate the regime model using local Markov distance functionals with corresponding
 87 time dependent probabilities (Horenko 2011a). In studies that look into forecasting of regimes on

88 sub-seasonal timescales, the probability of being in a regime is often considered by looking at the
89 empirical distribution of the (hard) regime assignment across an ensemble (Vigaud et al. 2018;
90 Cortesi et al. 2021; Büeler et al. 2021; Falkena et al. 2022). Such an approach is already used in
91 an operational setting by e.g. ECMWF (Ferranti et al. 2015). A limitation of this method is that it
92 requires availability of ensemble data, where typically the ensemble size is small, and verification
93 is done against a hard regime assignment from reanalysis.

94 A probabilistic regime assignment that does not require this availability of ensemble data would
95 help in better assessing the skill in predicting regimes, as it could be applied to reanalysis data which
96 is also subject to noise. Such a regime assignment would allow to identify the instances in which
97 the observations cannot be clearly assigned to one regime or in which a wrong hard assignment
98 is potentially due to noise. This approach allows for a fairer verification of the model by taking
99 some degree of observational uncertainty into account. Here it is desirable for the approach to be
100 sequential, which allows for the regime assignment to be done in real time making it suitable for
101 operational applications. Most probabilistic regime assignment methods, such as mixture models
102 or HMMs, require the availability of the full dataset when computing the regime probabilities,
103 which would mean one has to rerun the clustering algorithm whenever a new datapoint is added. A
104 method that, after training on an initial dataset, can easily be applied to data as it becomes available
105 is more suitable for an operational setting. Such a method can also be applied to predefined
106 regimes, to provide traceability with previous work.

107 The standard hard regime assignment can be considered as a random process that takes a value
108 in the set of possible regimes at each time. The associated probability can be computed on the
109 basis of metastability frequencies computed from previous or currently available batch data. The
110 aim is to determine the corresponding conditional probability of being in a regime given the data,
111 i.e. $P(\text{Regime}|\text{Data})$. Following Bayes Theorem this is given by

$$P(\text{Regime}|\text{Data}) = \frac{P(\text{Data}|\text{Regime})P(\text{Regime})}{P(\text{Data})}, \quad (1)$$

112 combining prior knowledge of the probability of being in a regime $P(\text{Regime})$ with an observed
113 likelihood given a regime $P(\text{Data}|\text{Regime})$. The latter can sometimes be computed from the
114 climatological data. In Figure 1(a) the observed (climatological) likelihood functions for both
115 regimes are shown next to the trajectory. The working of Bayes Theorem for such a trajectory is

116 shown in Figure 1(b), which shows how the inclusion of prior information $P(\text{Regime})$ following
117 Bayes Theorem (1) affects the posterior $P(\text{Regime}|\text{Data})$ for the trajectory at days 7, 8 and 9,
118 following a section along the dotted line in Figure 1(a). The climatological likelihood functions
119 of the two regimes A and B, indicated by the dashed lines, are weighted (solid lines) using the
120 prior regime probabilities, shown by the non-hatched bars at the edge of the panels. The posterior
121 probabilities are then computed as the values of the weighted likelihood functions at the datapoint
122 (vertical black line). The obtained Bayesian probabilities are indicated by the hatched bars and
123 used to inform the prior probabilities for the next timestep, using climatological information about
124 transition probabilities.

125 At day 7 the prior information indicates a very high probability of being in regime A as all previous
126 days belonged clearly to that regime. This increases the probability of $t = 7$ belonging to regime A
127 and decreases that of belonging to regime B with respect to the climatological likelihood, which
128 would otherwise be evenly balanced between the two regimes. Thus, there is a high probability
129 that the data at day 7 belongs to regime A. Given the known persistence of regimes, the prior
130 information for day 8 again then indicates a high probability of being in this regime, albeit slightly
131 smaller than at $t = 7$, which weights the likelihood functions accordingly. Although the data is
132 closer to regime B, the prior information means that there is an approximately equal probability of
133 being in either of the two regimes. The prior for $t = 9$ thus does not weight the likelihood functions
134 as much as for $t = 7$ and 8, and thus the data at day 9 being equally close to both regimes means
135 that again the probability of being in either of the regimes is close to a half. This discussion shows
136 how the inclusion of prior information can be used to compute the probability of a regime given the
137 data, and thereby soften the effects of noise, following the fundamental principles of probability
138 as encoded in Bayes Theorem (1). As noted above, the approach as discussed here is sequential
139 and can be applied to individual realisations, making it suitable for operational applications. An
140 initial training dataset can be used to obtain the climatological likelihood functions, after which the
141 regime assignment can be applied to data as it becomes available. The latter regime assignment
142 step is similar to finding the most probable sequence once a HMM is known (Viterbi 1967; Rabiner
143 1989).

144 Other aspects than persistence can affect the prior regime likelihood as well. It is likely that
145 non-stationary external factors, such as the El Niño Southern Oscillation (ENSO) or Sudden

146 Stratospheric Warmings (SSWs), have an influence on the prior regime probabilities (e.g. Toniazzo
147 and Scaife 2006; Ayarzagüena et al. 2018; Domeisen et al. 2020). The Bayesian approach allows
148 to incorporate such information, either by looking at e.g. an ENSO index or by making use of the
149 availability of ensemble data. In a previous study a regularised clustering method helped to identify
150 a more pronounced interannual regime signal by making use of the information available in an
151 ensemble (Falkena et al. 2022). Similarly, having a more informative prior for Bayes Theorem (1),
152 incorporating information from external processes, can help in identifying a stronger non-stationary
153 regime signal. The Bayesian approach discussed here is not the only method in which information
154 on external forcing can be incorporated in the regime assignment (e.g. Franzke et al. 2015), but it
155 is (to our knowledge) the first that allows to do this in a sequential manner.

156 In this paper we formalise the intuition of Figure 1 and study how to use Bayes Theorem to obtain
157 a probabilistic regime assignment based on predefined regimes for the wintertime Euro-Atlantic
158 sector. The use of predefined regimes respects the scientific value that has already been established
159 for those regimes, e.g. in the relationship with particular climate impacts. In Section 2 we discuss
160 the data that are used and the use of standard k -means clustering to obtain the circulation regimes
161 that we consider for this study. The two sections that follow explain the way in which Bayes
162 Theorem can be used for the regime assignment, where an important aim of our work is to link
163 our method to existing work on clustering of circulation regimes. We start with the most intuitive
164 sequential form (as discussed above) in Section 3 and in Section 4 we consider how the use of
165 ensemble data, which picks up some external forcing signals, can help to update the prior regime
166 probabilities to study interannual regime variability, which is discussed in Section 5. A discussion
167 and conclusion are given in Section 6.

168 **2. Data and Clustering**

169 For the identification of the circulation regimes the 500 hPa geopotential height fields (Z500)
170 from two datasets are used: the ECMWF SEAS5 hindcast ensemble dataset (Johnson et al. 2019)
171 and the ERA-Interim reanalysis dataset (Dee et al. 2011). For both datasets, daily (00:00 UTC)
172 gridpoint ($2.5^\circ \times 2.5^\circ$ resolution) Z500 data over the Euro-Atlantic sector (20° to 80° N, 90° W to
173 30° E) are considered for all winters (DJFM) for which the SEAS5 ensemble data are available
174 (1981-2016). The regimes are computed using gridpoint anomaly data, where the anomalies are

175 computed with respect to the average DJFM climatology (see Falkena et al. (2020) for the rationale
176 for this choice). Here the climatologies of ERA-Interim and SEAS5 are used as a reference for the
177 computation of their respective anomalies. The SEAS5 hindcast ensemble has 51 members and is
178 initialised each year on November 1st, which means that by considering data only from December
179 onwards the effect of the atmospheric initial conditions has been effectively lost. This allows us
180 to treat each ensemble member as an alternative, physically plausible yet not observed realisation
181 of the atmosphere (Thompson et al. 2017), subject to the non-stationary influences for that year
182 (notably ENSO).

183 A standard k -means clustering algorithm (Jain 2010), with a Euclidian distance to compute the
184 distance between the data and regimes, is used to identify six circulation regimes over the Euro-
185 Atlantic sector for both ERA-Interim and the SEAS5 hindcast ensemble. In k -means clustering the
186 data are sorted in k clusters that are close together within one cluster, but far from data in the other
187 clusters based on some distance measure. These clusters are represented by their mean, which
188 corresponds to the circulation regimes, where the number of clusters k has to be set a priori. Six
189 was identified as a suitable number of regimes for such unfiltered data in a previous study (Falkena
190 et al. 2020). The regimes for the SEAS5 hindcast ensemble are shown in Figure 2 and are the two
191 phases of the North Atlantic Oscillation (NAO), the Atlantic Ridge (AR), Scandinavian Blocking
192 (SB) and both their counterparts. Note that these regimes are slightly different in their patterns
193 from those of ERA-Interim (see Falkena et al. (2022) for details on this), thereby providing an
194 inherent bias correction between the model and reanalysis. These hard regime assignments are
195 used to compute the likelihood functions that are used in the Bayesian approach, for which a
196 detailed discussion is given in Section 3a. In addition we consider the (hard) regime assignments
197 obtained using the time-regularised clustering algorithm from Falkena et al. (2020). This allows
198 for a comparison of different approaches to identify the persistent regime signal.

199 **3. Sequential Bayesian Regime Assignment**

200 In this section the Bayesian approach to regime assignment is discussed, which can be applied to
201 ERA-Interim data as well as single ensemble realisations. We start with the details of the method
202 itself in Section a, followed by a comparison with the results of both a standard and time-regularised
203 k -means clustering method in Section b.

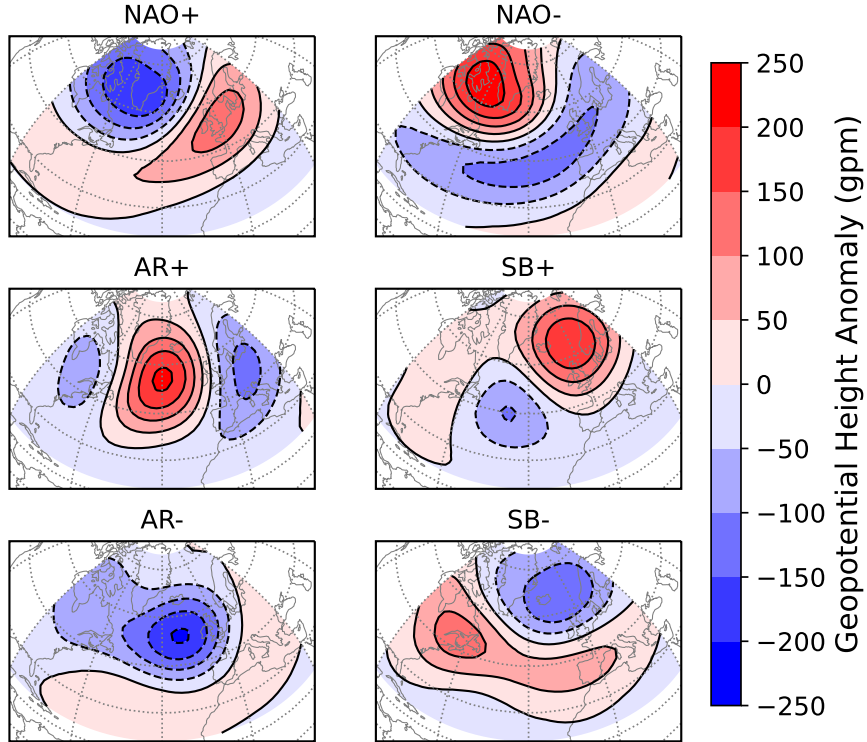


FIG. 2: The six circulation regimes obtained for the SEAS5 ensemble using k -means clustering. From top-left to bottom-right: 1. NAO+, 2. NAO-, 3. Atlantic Ridge (AR+), 4. Scandinavian Blocking (SB+), 5. AR-, 6. SB-.

204 *a. Method*

205 The starting point for our sequential Bayesian regime assignment is the six regimes obtained
 206 using k -means clustering discussed in Section 2 and shown in Figure 2. The likelihood functions
 207 in Bayes Theorem (1) are computed based on the distance to these regimes, and remain fixed
 208 throughout the sequential Bayesian regime assignment. The discussion of the method as phrased
 209 below is general, and can be applied to all types of regime dynamics as long as the regimes
 210 themselves and the likelihood functions are specified a priori.

211 Let r be a discrete random variable indicating a regime, i.e. taking values in $\{1, \dots, k\}$ for k
 212 regimes, and let $\mathbf{d} \in \mathbb{R}^k$ be a vector containing the distances to each of the regimes (here the Euclidian
 213 distance is used which is also the standard cost function in the k -means setting). Specifically, \mathbf{d}

214 are the data we consider in our Bayesian approach. The use of the regime distance as data is not
 215 the only option. When one considers only a limited number of principal components (PCs) for the
 216 regime representation the PC values can be directly used. However, for the spatial fields considered
 217 here (see Falkena et al. (2020) for the arguments in favor of using gridpoint data) this is unfeasible
 218 as the high dimensionality means the phase space is sparsely sampled leading to large uncertainty
 219 in the resulting distributions. Therefore, a means of dimension reduction is required for which
 220 we consider the distances to the different regimes since this is the metric used in most clustering
 221 approaches. At a given time we are interested in the probability to be in a regime r given the data,
 222 i.e. $P(r|\mathbf{d})$. Bayes Theorem tells us that

$$P(r|\mathbf{d}) = \frac{P(\mathbf{d}|r)P(r)}{P(\mathbf{d})}. \quad (2)$$

223 Here, $P(r)$ is the prior probability of regime r and $P(\mathbf{d})$ is the probability of the data. Since we
 224 only consider a discrete number of regimes which are mutually exclusive and exhaustive, the latter
 225 can be computed by

$$P(\mathbf{d}) = \sum_{r=1}^k P(\mathbf{d}|r)P(r), \quad (3)$$

226 making it a normalisation factor.

227 Lastly, $P(\mathbf{d}|r)$ is the likelihood of the data given a regime r . The likelihood of the data can
 228 be determined from the distance to each of the regimes by considering how the data fall within
 229 the conditional distance distributions, i.e. the distributions conditioned on data belonging to one
 230 of the regimes. For each datapoint in either the SEAS5 or ERA-interim timeseries we have this
 231 distance to each of the k regimes, which has been computed in the k -means clustering procedure
 232 to determine the hard regime assignment (Section 2). This gives the distributions of the distances
 233 to each of the regimes conditional on regime r , which for SEAS5 are shown in Figure 3.

234 There are a few things to note concerning these distributions. Firstly, the distance to the regime
 235 the data is assigned to is smallest, but can still be larger than the distance to other regimes for
 236 a different datapoint belonging to that regime. Secondly, for data assigned to AR+, SB+, AR-
 237 and SB- the distances to the other regimes are roughly equally distributed with the means being
 238 relatively close to each other. However, for data assigned to either NAO+ or NAO- the distance
 239 to the other phase is larger than that to the other four regimes. Thus these two regimes are further

240 away from each other than the rest of the regimes, and information on the proximity to one regime
 241 is providing information on the proximity to the other.

242 Also, we see that these distributions are approximately normal, justifying us to approximate
 243 the corresponding k -dimensional conditional probability density functions (pdf) by a multivariate
 244 normal. The likelihood $P(\mathbf{d}|r)$ is then given by the value of the conditional pdf, that is

$$P(\mathbf{d}|r) = \frac{-\frac{1}{2}(\mathbf{d} - \mu_r)^T \Sigma_r^{-1} (\mathbf{d} - \mu_r)}{\sqrt{(2\pi)^k |\Sigma_r|}}, \quad (4)$$

245 where $|\cdot|$ represents the determinant. The mean μ_r and covariance Σ_r , representing the variability
 246 around the cluster centre, are estimated from the conditional distance distributions obtained from
 247 the k -means clustering results for each regime. These estimates are done separately for ERA-
 248 Interim and SEAS5 to avoid biases due to the regimes being slightly different. The estimates of
 249 the mean and covariance are surprisingly similar between both datasets, indicating that, apart from
 250 the slight difference in regimes, the model does a reasonable job in representing the variability of
 251 the regime dynamics. A further discussion on this, including a robustness analysis of the distance
 252 distributions is given in the Supplementary Material.

253 To obtain the prior probability $P(r)$ there is a natural choice from propagating the probabilities
 254 of the previous timestep forward. From k -means clustering an estimate of the regime dynamics
 255 is known, which is characterised by the climatological regime frequencies P^c and transition
 256 probabilities T_{ij}^c between the regimes. For SEAS5 these are given by (Falkena et al. 2022) (for the
 257 regimes ordered as in Figure 2)

$$P^c = \begin{pmatrix} 0.176 \\ 0.158 \\ 0.160 \\ 0.163 \\ 0.175 \\ 0.168 \end{pmatrix}, \quad T^c = \begin{pmatrix} 0.728 & 0.000 & 0.039 & 0.062 & 0.060 & 0.112 \\ 0.000 & 0.822 & 0.050 & 0.046 & 0.053 & 0.029 \\ 0.079 & 0.054 & 0.702 & 0.075 & 0.021 & 0.069 \\ 0.069 & 0.058 & 0.065 & 0.739 & 0.037 & 0.031 \\ 0.072 & 0.032 & 0.035 & 0.045 & 0.771 & 0.045 \\ 0.065 & 0.033 & 0.095 & 0.029 & 0.070 & 0.708 \end{pmatrix}. \quad (5)$$

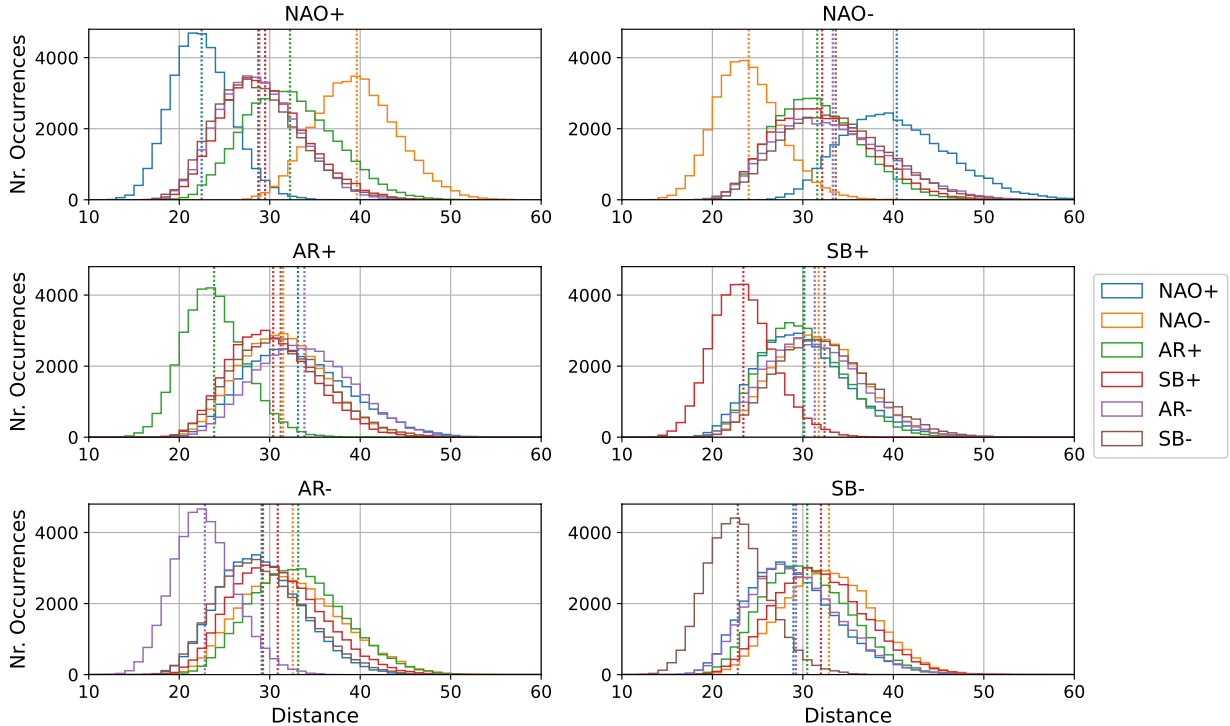


FIG. 3: The distributions of the distances (normalized, gpm/#gridpoints) to each of the regimes (color) conditional on the SEAS5 hindcast data being assigned to the regime given in the title, based on a hard assignment. The means of each distribution are indicated by the vertical dotted lines.

258 Starting from the regime probabilities at time $t - 1$, a best estimate of the prior probabilities for the
 259 next time step is

$$P(t) = T^c P(t-1|\mathbf{d}), \quad (6)$$

260 where $P(t)$ is the vector of prior probabilities $\{P(r)\}_{r=1,\dots,k}$ at time t and $P(t-1|\mathbf{d})$ the vector
 261 of posterior probabilities $\{P(r|\mathbf{d})\}_{r=1,\dots,k}$ at time $t-1$. Note that in the transition matrix T^c the
 262 diagonal elements — corresponding to persistence of the current regime — dominate. At the
 263 start of each winter, on December 1st, there is no previous probability to use, and thus little prior
 264 information on the probability of being in any of the regimes. For that reason the climatological
 265 regime frequencies P^c are used as a prior. Note that this is nearly as uninformative as using a
 266 uniform distribution. Here the hard regime assignment is used to obtain both the initial prior for
 267 each winter and the transition probabilities to obtain subsequent priors. This is by no means the

268 only option, e.g. one could also use a uniform prior at the start of winter. The choice made here is
269 closest to existing methods and therefore least biased when comparing the results.

270 Using the prior probabilities $P(r)$ and likelihood of the data $P(\mathbf{d}|r)$ following the conditional
271 distance distributions we can compute the posterior Bayesian probability of a regime given the data
272 $P(r|\mathbf{d})$ using Bayes Theorem (2) in every timestep. This yields a sequential probabilistic regime
273 assignment, where the regime probabilities of one day are used to obtain a prior for the next day.
274 Applying this method to ERA-Interim data and the ensemble members of the SEAS5 ensemble
275 yields a probability of being in each of the six regimes at every day in winter. From here on we refer
276 to this posterior Bayesian probability simply as the Bayesian probability. This Bayesian approach
277 can be related to a HMM approach, where the regime patterns and their transition probabilities are
278 given a priori, leaving only the hidden regime assignment to be discovered. Here the used likelihood
279 differs from that commonly used in the standard Expectation-Maximization (EM) algorithm (e.g.
280 Dempster et al. 1977; Rabiner 1989). In case the transition matrix T cannot be obtained directly,
281 as is done here through observation of the hard regime assignment, one could employ techniques
282 to find T via algorithms designed in the context of HMMs.

283 The above described sequential Bayesian regime assignment is simple and allows for a straightfor-
284 ward comparison with the commonly used hard regime assignment, as well as with the regularised
285 clustering results (without the need of selecting a constraint parameter). However, there are other
286 options to model the uncertainty and to update the corresponding model parameters sequentially.
287 For instance one can model each regime individually and associate its center estimates with the
288 mean of a Gaussian. The updating procedure for such a model is called the Kalman filter (Kalman
289 1960) or the corresponding Monte Carlo approximation the Ensemble Kalman Filter (Evensen and
290 van Leeuwen 2000), and of course various other methods for more general distributions as well as
291 iterative assimilation of incoming information exist (e.g. Kantas et al. 2014; Hu and van Leeuwen
292 2021; Acevedo et al. 2017). The method used here is closer to a particle filter (Del Moral 1997;
293 Doucet et al. 2001) as our ensemble members are weighted with importance weights stemming
294 from the likelihood rather than using an analytic formula such as is used in the Kalman filter.
295 However, in this paper we specifically aim to stay close to existing methods and model the process
296 of hard regime assignments as random variables in each time step. This allows for a straightforward
297 implementation which can be readily applied in an operational setting. Furthermore, using this

298 method we can investigate whether the results are comparable to those found using regularised
299 clustering methods, which have been used to improve the regime persistence in the identification
300 procedure, without the need to select a constraint parameter.

301 *b. Evaluation*

302 The first question to answer is what the effect is of this Bayesian approach in practice, and whether
303 this matches the intuition behind the method. How does the prior affect the Bayesian probabilities?
304 A next step is to compare the probabilistic approach with results obtained using a hard regime
305 assignment, as given by k -means clustering. Is the average regime frequency affected? What is
306 the effect on the regime persistence? In this section we start by discussing the first question by
307 looking at some examples to get a sense for how the method is working in practice, after which we
308 look at the statistics of the results compared to a k -means clustering approach to answer the other
309 questions.

310 To start, we consider the Bayesian regime probabilities for a single randomly chosen ensemble
311 member. As the sequential Bayesian regime assignment works on a single-member basis this is
312 the best way to gain insight into the workings of the Bayesian method. In Figure 4 the prior
313 and Bayesian regime probabilities for the 23rd ensemble member are shown together with the
314 climatological likelihood corresponding to the observed datapoint. A first aspect to note is that
315 most of the time the regime likelihood $P(\mathbf{d}|r)$ gives a clear indication of the regime the data
316 belong to. Secondly, we see that the prior quite closely follows the Bayesian probabilities with
317 a delay of one day, corresponding to the high persistence in the transition matrix (Equation (5)).
318 The initial prior, given by the climatological values, is uninformative and in that case the regime
319 likelihood nearly fully determines the Bayesian probabilities. Subsequently, the prior is much more
320 informative but in most cases the regime likelihood still strongly determines the final probability.
321 However, when the likelihood does not clearly point towards one regime, e.g. around days 8-12,
322 the prior information shifts the probabilities towards stronger persistence, in this case of the AR+
323 regime. This can also be seen around day 99-101, corresponding to days 7-9 in the example shown
324 in Figure 1 in Section 1, where the inclusion of prior information favors persistence over a short
325 excursion away from the most likely regime. In this way the Bayesian regime assignment allows
326 for identifying stronger persistence, i.e. high probability of the dominant regime, without losing

327 the signal of other regimes entering the dynamics as they still have some non-zero probability. The
 328 effect of this approach for ERA-Interim data is similar.

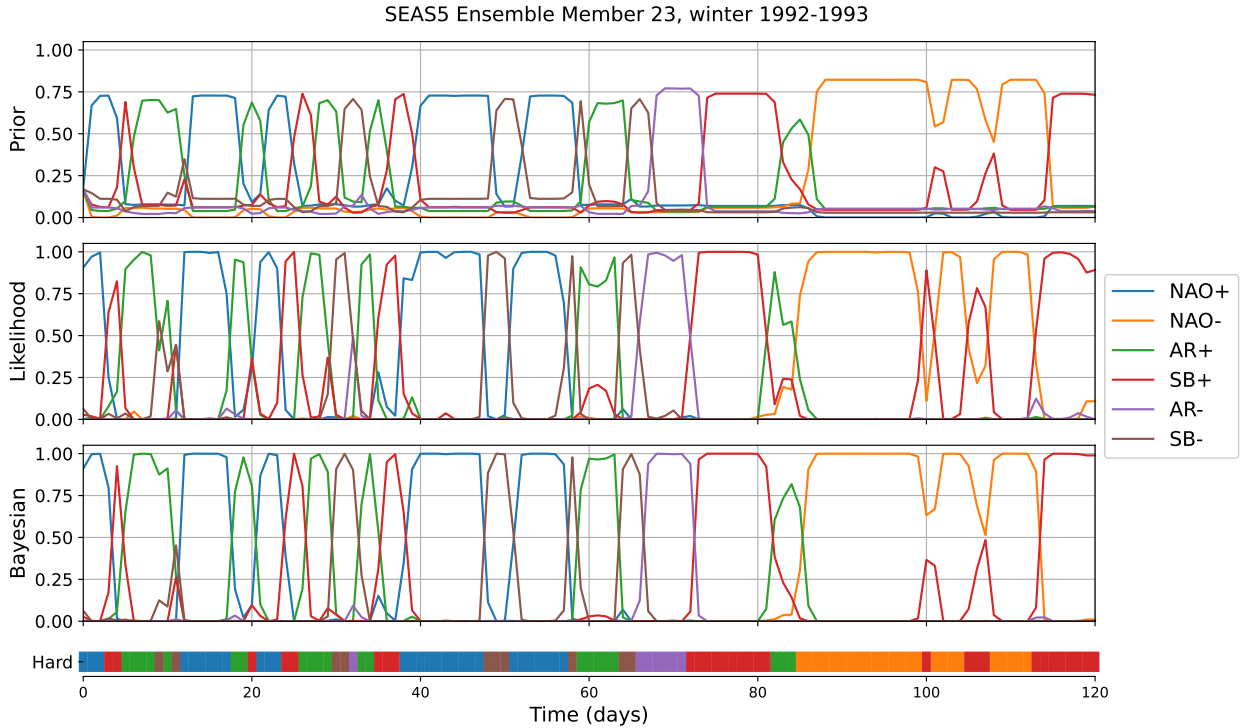


FIG. 4: The prior probability, conditional regime likelihood and Bayesian regime probability for the 23rd ensemble member in the sequential Bayesian regime assignment procedure for the winter of 1992-1993. The bar at the bottom indicates the hard regime assignment following k -means clustering.

329 The Bayesian probabilistic regime assignment allows to understand some of the subtleties of
 330 the regime dynamics, e.g. regime transitions occur in the form of a decrease/increase of the
 331 regime probabilities. How does such an approach compare to the commonly used hard regime
 332 assignment obtained using k -means clustering? The bar at the bottom of Figure 4 shows the
 333 hard regime assignment corresponding to this time series. The Bayesian regime probabilities
 334 vary more smoothly, and show less short back-and-forth transitions between regimes which occur
 335 several times for the hard regime assignment, e.g. around day 9 and 20. In Falkena et al.
 336 (2020) a constraint on the number of transitions between regimes was introduced to reduce the
 337 number of short back-and-forth transitions between regimes, based on the regularised clustering
 338 method introduced by Horenko (2010). This was shown to increase the regime persistence without
 339 affecting the regime occurrence rates, provided the constraint parameter was chosen appropriately.

340 The optimal constraint parameter corresponded to an average regime duration of 6.3 days. It was
341 selected by considering the Bayesian Information Criterion and falls within the region where the
342 regime occurrence rates are not affected by the regularisation.

343 In Figure 5 a comparison between the regime likelihood, Bayesian regime probabilities and
344 a hard regime assignment obtained using either a standard or regularised k -means approach is
345 shown for ERA-Interim for the winter of 1993-1994. The regularisation does reduce the number
346 of regime transitions, by e.g. removing the NAO+ regime between two occurrence of SB- around
347 day 18. At the same time the Bayesian probabilities show a small increase in the NAO+ likelihood,
348 with SB- still having the highest probability. Here the regularisation and Bayesian approach
349 thus yield similar results. On the other hand, around e.g. day 84 and 107 the regularisation
350 eliminates some regime transitions where the Bayesian probabilities still show some signal of
351 the corresponding regimes. The probabilistic approach thus allows to identify the data where
352 the regime assignment is less clear, showing an increase in probability instead of a hard regime
353 change. It also retains some regime transitions that the regularised clustering eliminates due to
354 it being difficult to select the “correct” constraint value. In the probabilistic approach these show
355 as increases in the corresponding regime probability. This analysis confirms that the Bayesian
356 approach seems to be doing something sensible, without having to tune any parameters. When the
357 data clearly belongs to one of the six regimes, there is little benefit to the Bayesian approach. The
358 main times where it makes a difference are the periods when one regime transitions into another, or
359 when a regime loses some of its strength in favor of another regime but then gains in strength again.
360 Such a reduction in the regime probabilities could be an indication of increased flow instability,
361 being close to transitioning into another of the six canonical states.

362 The impact of the sequential Bayesian approach on the regime frequencies, computed as the
363 average Bayesian regime probability for this method, and (1-day) autocorrelation is shown in
364 Figure 6. Here the autocorrelation for the hard regime assignment is computed using a time series
365 which is one when data is assigned to the corresponding regime and zero otherwise. The average
366 frequencies of the regimes do not change when using the Bayesian regime assignment, as can be
367 seen in Figure 6(a). This holds both for the SEAS5 hindcast ensemble data and for ERA-Interim,
368 where also the results of the regularised k -means clustering algorithm are shown for comparison.
369 On the other hand the autocorrelation, being an indication of the persistence of the regimes, is

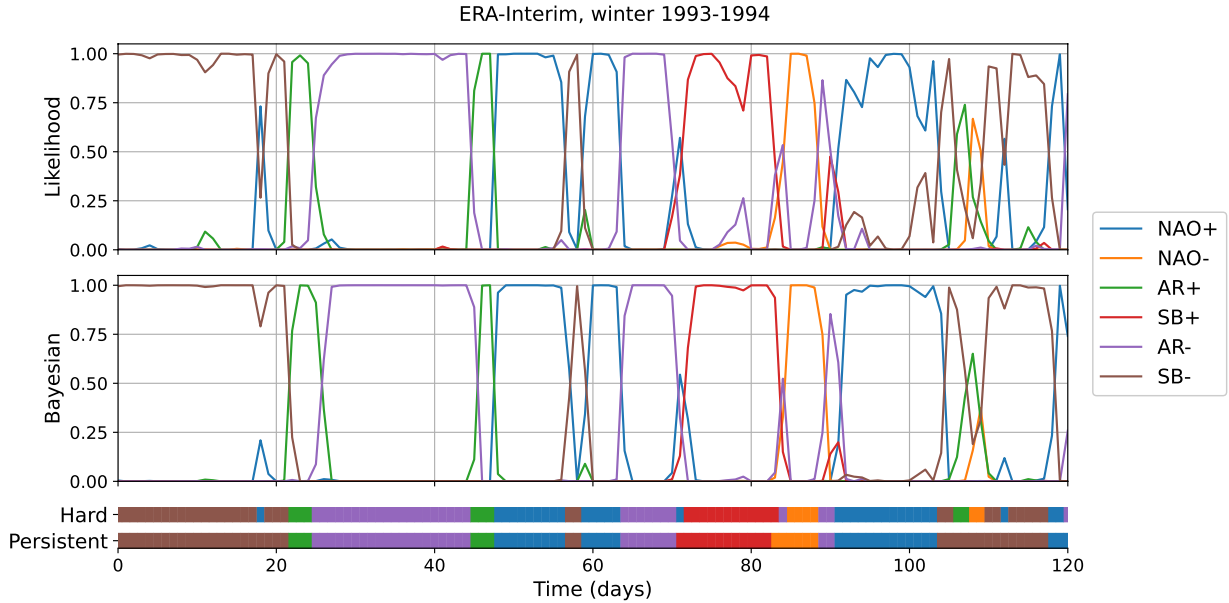


FIG. 5: The observed regime likelihood and Bayesian regime probability for ERA-Interim, with the hard assignment using a standard or time-regularised (persistent) k -means algorithm shown by the bars for the winter of 1993-1994.

370 strongly affected (Figure 6(b)). For ERA-Interim we see that the sequential Bayesian approach
 371 increases the autocorrelation even beyond that obtained using a regularised clustering algorithm
 372 that contains a persistence constraint. Also for SEAS5 a strong increase in autocorrelation is found
 373 using the sequential Bayesian regime assignment compared to a standard hard assignment. For
 374 most regimes the ERA-Interim values lie at the top of the SEAS5 autocorrelation range, both for
 375 the standard and Bayesian approach. Thus we find that the Bayesian approach does not alter the
 376 regime frequencies, but does lead to more persistent regime dynamics, as we might hope. This
 377 suggests that the transition probabilities in Equation (5), which are used to obtain the prior regime
 378 probabilities, likely are an underestimation of the true persistence, which is improved by the use of
 379 Bayes Theorem.

380 4. Ensemble Bayesian Regime Assignment

381 The implicit assumption made in the sequential Bayesian approach as discussed in the previous
 382 section is that the regime dynamics is statistically stationary in time. That is, the climatological
 383 likelihood functions and transition probabilities do not change in time. This is a reasonable and
 384 minimal first assumption yielding good results, but it is likely that external factors such as ENSO

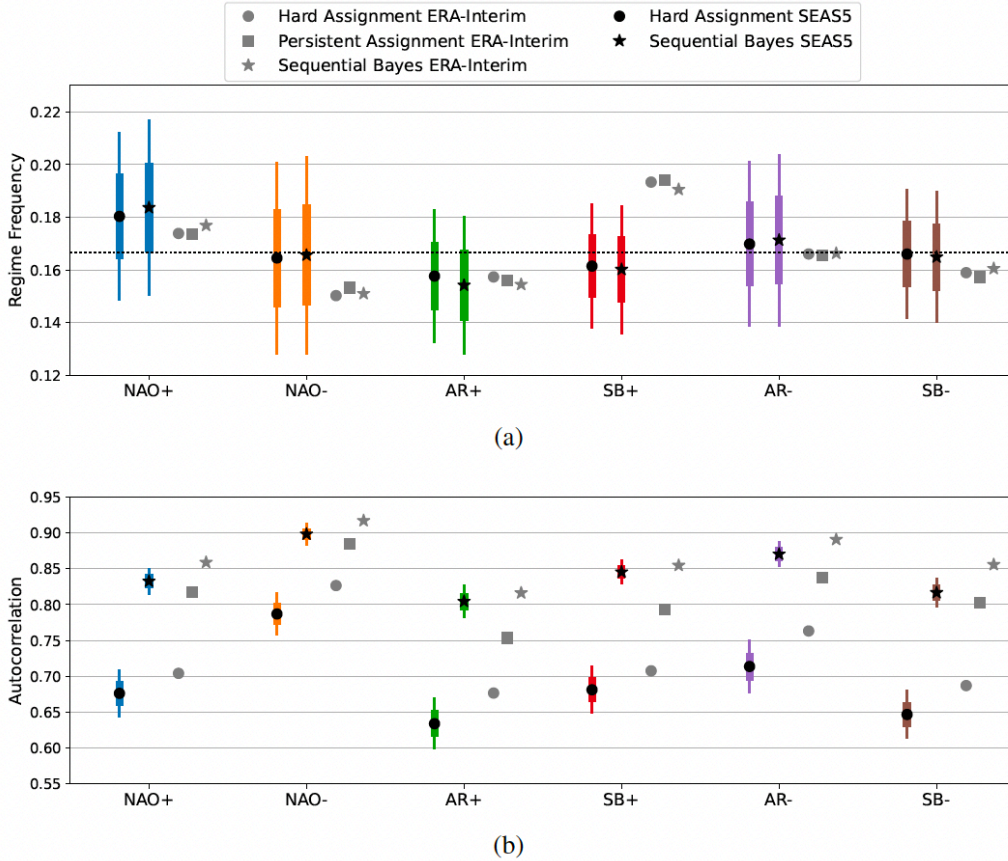


FIG. 6: The regime frequencies and 1-day autocorrelation as obtained using either standard k -means clustering (circles) or a sequential Bayesian regime assignment (stars) for the SEAS5 hindcast ensemble (symbols with error bars) and ERA-Interim (symbols only), for which also the values obtained with the time-regularised k -means clustering method are shown (squares). Error bounds are determined using bootstrapping with one member per year (with replacement, 500 times), where the thick bars indicate the plus-minus one standard deviation range with thin bars extending showing the 95% confidence interval.

385 affect some aspects of the regime dynamics as discussed in Section 1. There are two obvious ways
 386 in which to include the effect of external forcing in the Bayesian approach. The first is to update
 387 the regime likelihood functions in time. The second is to update the prior probabilities. These two
 388 aspects are by no means the only aspects of the regime dynamics that can be affected by external
 389 forcing. For example, one can imagine that the regimes themselves change as a consequence
 390 of external factors causing changes in the climate system. However, this is nearly impossible to
 391 quantify with the limited available data and no robust evidence for this has been found so far (e.g.
 392 Corti et al. 1999; Dorrington et al. 2022). Therefore, we only discuss the above-mentioned two
 393 approaches.

394 In the following analysis we focus on the latter of these two approaches. The main reason for
 395 this is the lack of data availability. Even though the SEAS5 hindcast ensemble has 51 members for
 396 each year, this still is insufficient to allow for e.g. weekly updating of the likelihood functions. An
 397 option for which sufficient data are available would be to compute the likelihood function during
 398 e.g. strong El Niño years, and use those to change the likelihood functions each year. However,
 399 this relies on the hypothesis that the regions in phase space belonging to each of the regimes shift
 400 as a consequence of ENSO forcing, while it may simply be the case that some regions are visited
 401 more often than others. As there are only 36 years of data available it is impossible to test this
 402 hypothesis and thus we refrain from pursuing this approach further. On the other hand, there is
 403 sufficient data to update the prior probabilities in time. There are several ways in which this can be
 404 done. For example, one can use information on ENSO to shift the prior probabilities, or one can
 405 make use of the ensemble information by allowing the transition probabilities to change in time.
 406 We pursue the latter approach, as it makes use of the information within the SEAS5 ensemble and
 407 does not require any external information. It is explained and evaluated in the next two sections
 408 followed by an analysis of the resulting interannual variability in Section 5.

409 *a. Updating the Transition Probabilities*

410 To obtain more informative prior regime probabilities, the transition probabilities T_{ij} from regime
 411 i to j are updated following the ensemble behavior. This allows not only for (fixed) persistence
 412 to inform the prior, but also non-stationary external factors, such as ENSO, through the ensemble
 413 statistics. Although there is not sufficient data to robustly estimate the transition probabilities
 414 directly, they can be inferred from the occurrence rates. The main assumption we make when
 415 updating the transition matrix T in time is that the regime probabilities are approximately stationary
 416 with respect to the current best estimate of the transition matrix. That is, we look for a transition
 417 matrix $T(t)$ for which the regime probabilities averaged over the ensemble at time t , $\bar{P}(t)$, are
 418 approximately stationary:

$$T(t)\bar{P}(t) = \bar{P}(t) + \epsilon^t. \quad (7)$$

419 Here ϵ^t is a noise term. Note that the climatological transition probabilities P^c are (nearly)
 420 stationary with respect to the transition matrix T^c . The aim thus is to find a transition matrix $T(t)$
 421 for which Equation (7) holds. In addition we have that a transition matrix is normalised, meaning

422 its columns each sum to unity:

$$\sum_{i=1}^k T_{ij} = 1, \quad \forall j \in 1, \dots, k. \quad (8)$$

423 This gives two equations which are used to update $T(t)$ at each timestep t . The problem of finding
 424 the values of the transition matrix $T(t)$ is ill-posed as there are not sufficient constraints, which
 425 means some choices need to be made in determining its values. The approach we propose in the
 426 following paragraph is one that follows the regime dynamics closely and is least biased in the sense
 427 that the deviations from T^c are equally distributed over all six regimes.

428 The regime dynamics is dominated by persistence, i.e. the probability of a regime to transition
 429 to itself corresponding to the diagonal elements of the transition matrix, as can be seen in Equation
 430 (5). Therefore we focus on these diagonal elements $T_{ii}(t)$ for updating the matrix $T(t)$ in time.
 431 Writing out Equation (7) elementwise while separating the diagonal and off-diagonal elements
 432 yields

$$T_{ii}(t)\bar{P}_i(t) + \sum_{j \neq i}^k T_{ij}(t)\bar{P}_j(t) = \bar{P}_i(t) + \epsilon_i^t, \quad \forall i \in 1, \dots, k. \quad (9)$$

433 As the diagonal terms dominate, we assume the off-diagonal elements do not differ much from the
 434 climatological values, that is $T_{ij}(t) \approx T_{ij}^c$ for all $i \neq j$. This yields an approximate equation for the
 435 diagonal elements of $T(t)$:

$$T_{ii}(t)\bar{P}_i(t) \approx \bar{P}_i(t) - \sum_{j \neq i}^k T_{ij}^c(t)\bar{P}_j(t). \quad (10)$$

436 When a particular regime is less populated than it is in climatology, the other regimes will
 437 conversely be more populated, implying a larger negative term on the right-hand side of (10) and
 438 thus a smaller value of the self-transition probability, which makes physical sense. Note that this
 439 approximation breaks down when $\bar{P}_i(t)$ is very small compared to the other $\bar{P}_j(t)$, in which case
 440 we set $T_{ii}(t) = 0$ to prevent negative values. Starting from the updated diagonal elements, the off-
 441 diagonal elements are computed using Equation (8) with an equal distribution of the perturbation
 442 from the climatological value over the off-diagonal terms.

443 The estimation of the transition matrix T in essence is the same as trying to fit a HMM to the
 444 data. The difficulty here is the limited availability of data, where we only consider data at one
 445 point in time to retain the sequential nature of the method. This makes the use of less heuristic,
 446 more sophisticated methods unreliable due to the large impact of noise on the data. If many
 447 more ensemble members would be available, something like the Baum-Welch algorithm might be
 448 a worthwhile approach for estimating T (Baum et al. 1970). Starting the updating of $T(t)$ from
 449 the diagonal elements and adjusting the off-diagonal elements equally is not the only option. It
 450 might even be better to not adjust the off-diagonal elements equally. However, since $\bar{P}(t)$ is an
 451 average over only 51 ensemble members, robustness would be an issue when making any further
 452 assumptions in updating $T(t)$ and hence we stick to the simplest approach.

453 The above method is equivalent to considering $T(t)$ as the climatological transition matrix plus
 454 a perturbation, i.e. $T(t) = T^c + T'(t)$, and subsequently assuming that the perturbations to the
 455 off-diagonal terms are small. An alternative way of looking at this is by considering it as a Markov
 456 regression model (Hamilton 1989; Krolzig 1997). That is, we write the transition matrix T as

$$T(t) = T^c + \sum_m \alpha_m(t) T_m. \quad (11)$$

457 Here T_m are matrices that set the shape of the perturbations to the climatological transition matrix,
 458 where the sum over each of the columns is zero for every m , and $\alpha_m(t)$ gives the strength of that
 459 term at time t . For a choice of

$$T_m = \begin{pmatrix} 0 & \dots & -\frac{1}{k-1} & \dots & 0 \\ & & \vdots & & \\ \vdots & & 1 & & \vdots \\ & & \vdots & & \\ 0 & & -\frac{1}{k-1} & & 0 \end{pmatrix}, \quad (12)$$

460 where the m -th column is non-zero this is exactly equivalent to the approach mentioned before.
 461 Here the α_m can be computed using the same assumptions as discussed before. This shows that
 462 there are several ways of looking at the problem that yield the same outcome, increasing the
 463 confidence in this approach.

464 *b. Evaluation*

465 To get an idea of how this approach can inform the prior probabilities consider Figure 7, which
466 shows both the sequential and ensemble Bayesian regime assignments for the (randomly chosen)
467 42nd ensemble member during the winter of 1992-93. This is the same winter for which the 23rd
468 ensemble member is shown in Figure 4. As an example, consider the probability of AR-. Around
469 days 5-10 the ensemble indicates this regime is less likely, as shown by a lower self-transition
470 probability, lowering the prior probability of the regime. On the other hand, from day 25 onward
471 AR- is more likely according to the ensemble, increasing its prior probability compared to the
472 sequential approach. In most cases changes to the final probabilities are small. The only exceptions
473 occur when a regime is deemed very unlikely, i.e. does not occur in any of the other ensemble
474 members, as happens twice for the SB+ regime between day 60 and 90. In these two cases a high
475 observed likelihood for SB+ is reduced substantially in the Bayesian probabilities in favor of the
476 second most-likely regime according to the likelihood, e.g. a 90% likelihood is reduced to a 35%
477 Bayesian probability. Yet importantly, the Bayesian probability of this regime is still non-zero, so
478 it can quickly respond to new information. The overall regime frequencies and autocorrelation are
479 not affected and remain as shown in Figure 6 for the sequential approach.

480 **5. Interannual Variability**

481 The interannual variability as obtained using the ensemble Bayesian regime assignment is shown
482 in Figure 8, with the result of the sequential Bayesian approach shown for reference (the interannual
483 variability of the sequential Bayesian approach is nearly identical to that obtained for the *k*-means
484 clustering assignment). The primary signal in the variability is found during very strong El Niño
485 years (vertical red solid lines) with SB- and NAO- showing an increase in frequency, while AR+,
486 AR- and NAO+ show a decrease in frequency. The signal during strong La Niña years (vertical
487 blue dash-dotted lines) is less clear, with on average an increase in NAO+ and decrease of NAO-
488 frequency. However, not every individual event matches this behavior. To define El Niño and La
489 Niña years the Niño 3.4 index is used (Trenberth 1997). Strong years correspond to a threshold of
490 ± 1.5 , and very strong years to a threshold of ± 2 . The asymmetry in the thresholds used for El Niño
491 and La Niña years is due to there being no very strong La Niña events in the considered time period.
492 These results, with a less pronounced regime response to La Niña compared to El Niño, reflect the

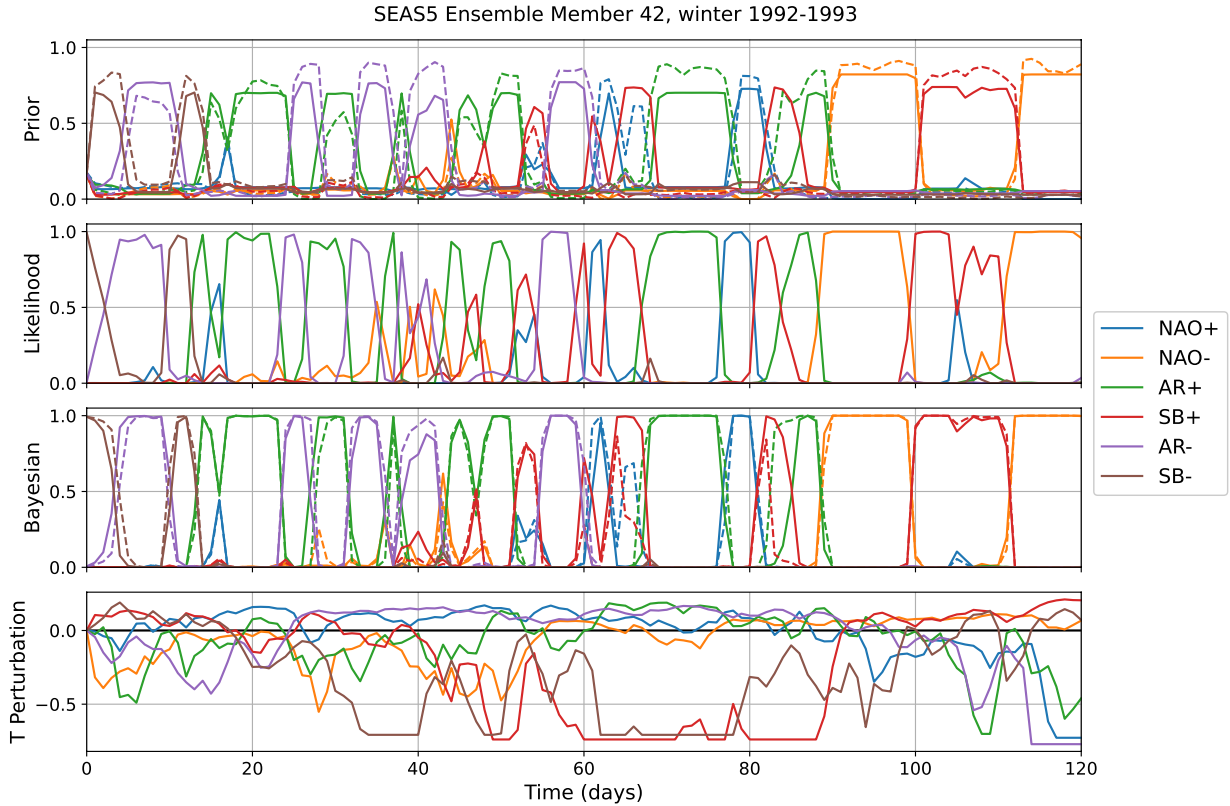


FIG. 7: In the top three panels the prior probability, conditional regime likelihood and Bayesian regime probability for the 42nd ensemble member in the Bayesian regime assignment procedure for the winter of 1992-1993 are shown. The solid line shows the sequential Bayesian approach and the dashed line the ensemble approach discussed in this section. The bottom panel shows the difference between the updated self-transition probabilities in the ensemble approach and the climatological values.

493 well-known nonlinearity of the response to ENSO (Straus and Molteni 2004; Toniazzo and Scaife
 494 2006) and are in line with those obtained in Falkena et al. (2022) using a regularisation on the
 495 ensemble members. The boxes on the right of each panel show the average regime frequencies
 496 during the identified El Niño and La Niña years for both the sequential and ensemble Bayesian
 497 approach, where there is an asymmetric response to ENSO for both methods. Some enhancement
 498 of the signal is found using the ensemble Bayesian regime assignment, which is most clear for the
 499 AR- and SB- regimes. The ERA-Interim variability from the sequential Bayesian approach is
 500 shown as well to give a perspective on the magnitude of the interannual variability.

501 To further consider the effect the updating of the transition matrix in the ensemble approach has
 502 on the interannual variability, consider Figure 9 which shows the difference between the sequential

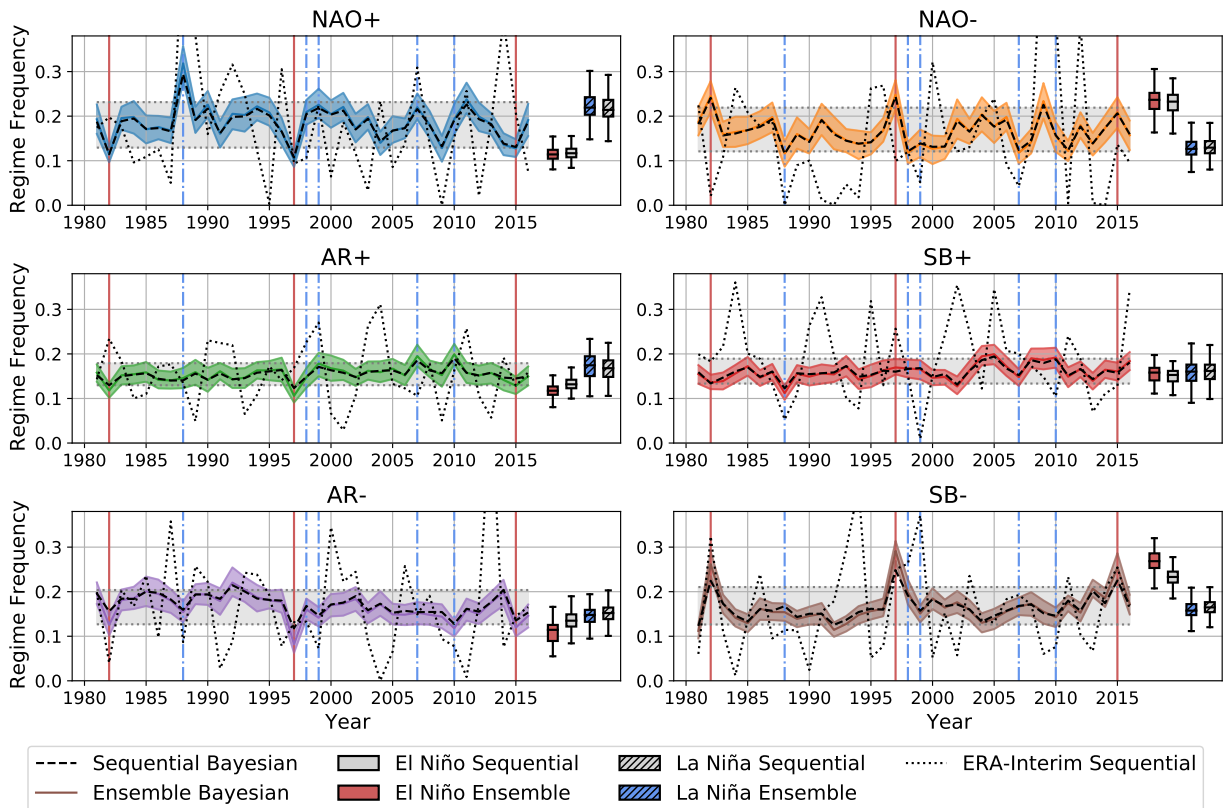


FIG. 8: The interannual variability of the occurrence rates for the ensemble Bayesian regime assignment for SEAS5 (color, with 95% confidence interval shaded), with the sequential Bayesian approach indicated by the black dashed lines. The grey shaded areas bounded by the grey dotted lines indicate the 10th and 90th percentile of the ensemble Bayesian assignment for each regime. The black dotted curve shows the ERA-Interim variability and the box-and-whisker plots on the right show the average occurrence rate during very strong El Niño (indicated by the vertical red solid lines) and strong La Niña years (indicated by the vertical blue dash-dotted lines).

503 and ensemble Bayesian regime assignment as well as the yearly average change to the self-transition
 504 probabilities, or persistence, of the regimes following the ensemble approach. Note that on average
 505 the perturbation to the self-transition probabilities is negative. The effect of the ensemble Bayesian
 506 approach on the regime frequencies is clearly visible for AR+, AR- and SB-, where the signal in
 507 response to El Niño is enhanced. For NAO+ a strong increase in regime frequency is found for the
 508 1988-1989 La Niña, together with a weak change during El Niño years. NAO- and SB+ do not
 509 show much difference in interannual variability between the two methods, although in the latter
 510 case there is little signal to enhance. The changes in the self-transition probabilities in general
 511 match those found in the regime frequencies, as expected. One aspect to note here is that for

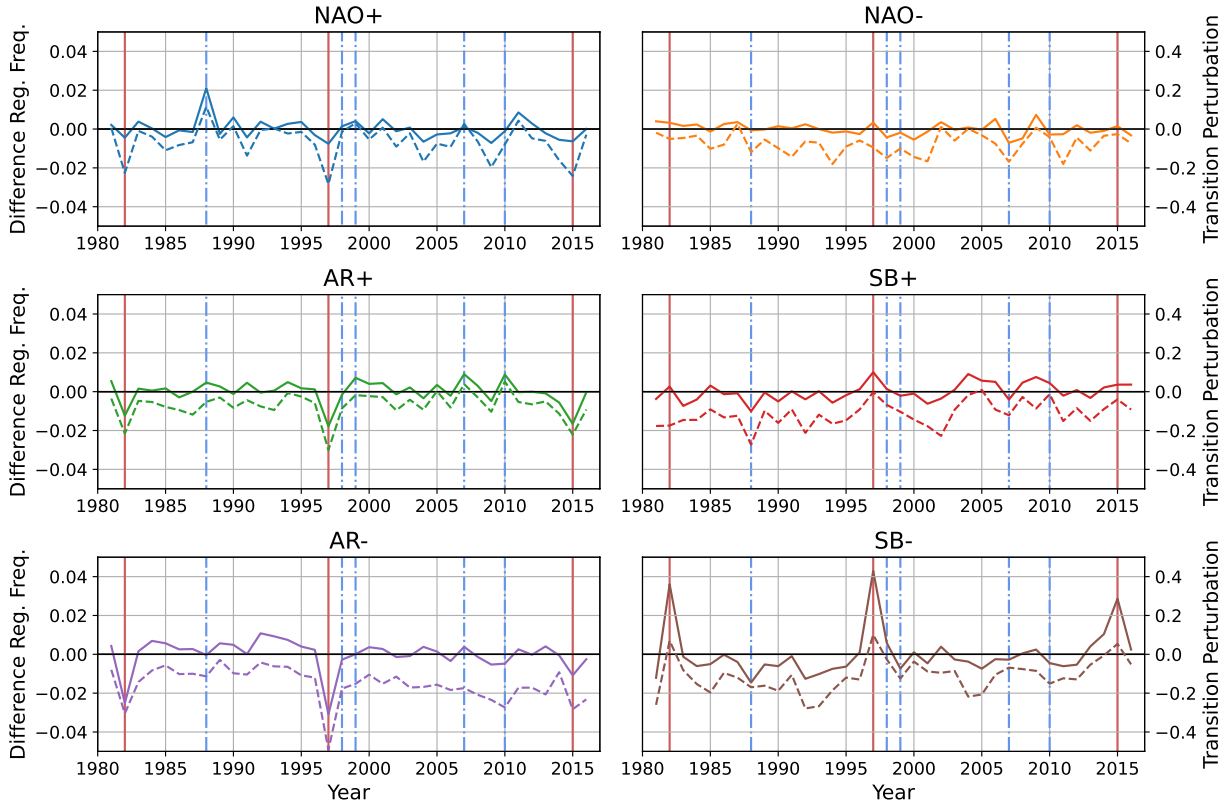


FIG. 9: The difference in interannual variability of the occurrence rates between the standard and ensemble Bayesian regime probabilities (solid), as well as the change in the self-transition probability for the regimes following the ensemble (dashed).

512 NAO+ the changes in the self-transition probability are relatively larger than those in the regime
 513 frequencies, especially when comparing to SB-.

514 The response of the changes in regime frequency to El Niño events found using the ensemble
 515 Bayesian approach appears to show a true signal and is very unlikely to have arisen by chance.
 516 To understand this, consider the change in regime frequency for SB-. The marginal probability
 517 of a very strong El Niño event is $3/36$ (3 events in 36 years), so the chance of the first increase
 518 in SB- frequency aligning with El Niño is $3/36$. Then, given the first El Niño event has already
 519 happened, the probability of the second spike aligning is $2/35$ and for the third $1/34$. This gives
 520 a probability of $3/36 \cdot 2/35 \cdot 1/34 \approx 10^{-4}$ for the alignment occurring by chance. The alignment
 521 of the increase/decrease in frequency for the other regimes only further decreases the probability
 522 of this being by chance. Also note that the response of both AR+ and AR- is a decrease in

523 regime frequency during El Niño years, indicating another aspect of nonlinearity in the circulation
524 response to ENSO.

525 Some of these signals in response to ENSO can already be picked up using 10-member ensembles.
526 In Figure 10 the interannual variability of the regime frequency is shown for 50 random 10-member
527 ensembles obtained from the full SEAS5 ensemble. For the full ensemble the strongest signal was
528 found for SB– during very strong El Niño years, and this is the signal that jumps out most strongly
529 again. To quantify this the Probability of Detection (POD) and False Alarm Ratio (FAR) for the
530 10-member ensembles are considered for peaks or troughs in regime frequency aligning with El
531 Niño and La Niña (Figure 11). Here, peaks and troughs are considered as exceedances with respect
532 to the n th percentile. The POD is computed as the number of peaks/troughs aligning with El
533 Niño/La Niña years over the total number of El Niño/La Niña years, and the FAR is computed as
534 the number of peaks/troughs outside those El Niño/La Niña years divided by the total number of
535 peaks/troughs. As expected, for El Niño there is a high POD for peaks in the SB– regime frequency
536 with a relatively low FAR (Figure 11(a)). Also for NAO– (peaks), NAO+, AR+ and AR– (troughs)
537 there is some signal, with the FAR being comparable to the POD. For La Niña years there is some
538 signal for NAO+, AR+ (peaks) and NAO– (troughs), but it is not as strong as for SB– in El Niño
539 years (Figure 11(b)). This is to be expected as we cannot expect to identify strong signals using a
540 smaller ensemble if they are not clear in the full ensemble. Nevertheless, the relatively high PODs
541 for these three regimes are encouraging.

542 To see whether the found response to ENSO for some regimes also reflects a predictable signal
543 in the observations we regress the ERA-Interim interannual variability onto the SEAS5 one, as
544 in Falkena et al. (2022). The results for this, looking at the sequential and ensemble Bayesian
545 approach, are shown in Table 1. In addition to the p -value, we also compute the Bayes factor
546 which is the ratio of the probabilities of the data given two different hypotheses H_1 and H_2 , i.e.
547 $P(D|H_1)/P(D|H_2)$ (Kass and Raftery 1995). Here the first hypothesis H_1 is that of a linear
548 regression model, whereas the second hypothesis H_2 assumes a constant, climatological, regime
549 frequency. For its computation we follow the Bayesian Information Criterion approximation from
550 Wagenmakers (2007). Values of the Bayes factor above one indicate H_1 is more likely, with
551 values between 3 and 20 constituting positive evidence and values over 20 yielding strong evidence
552 towards it (Kass and Raftery 1995).

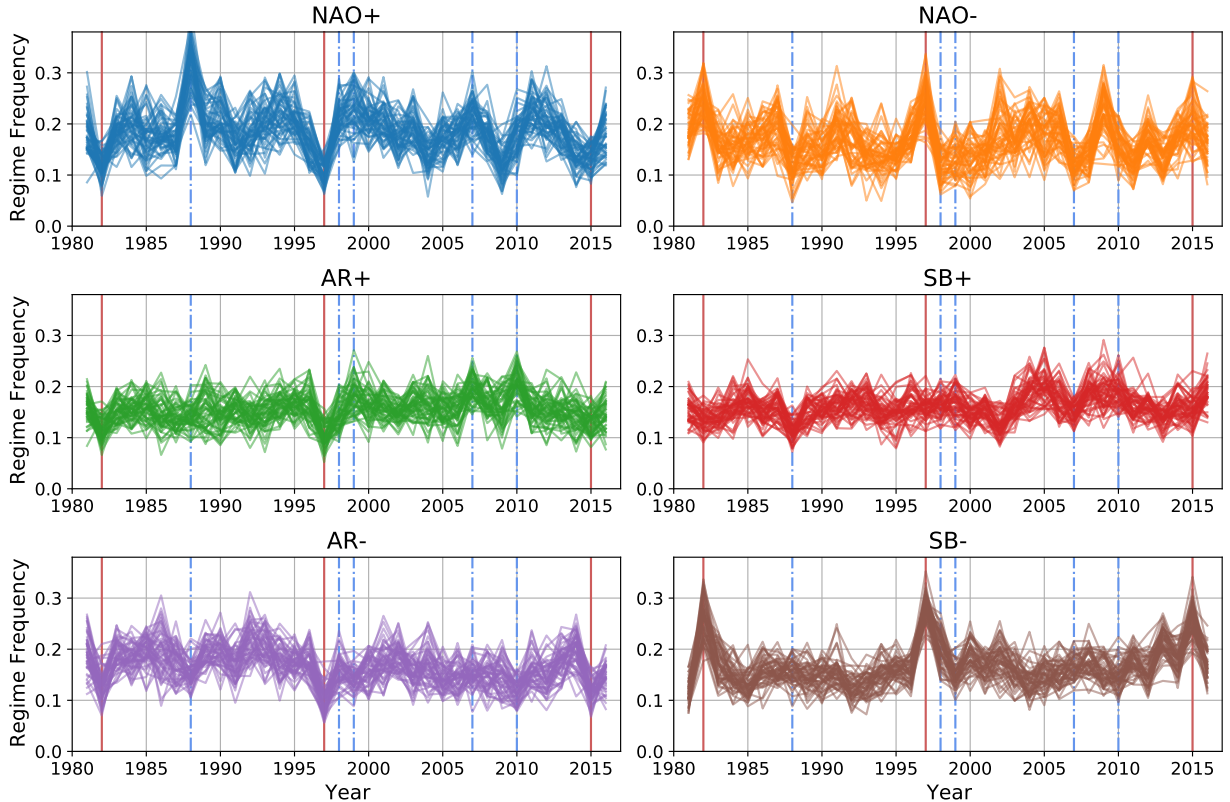
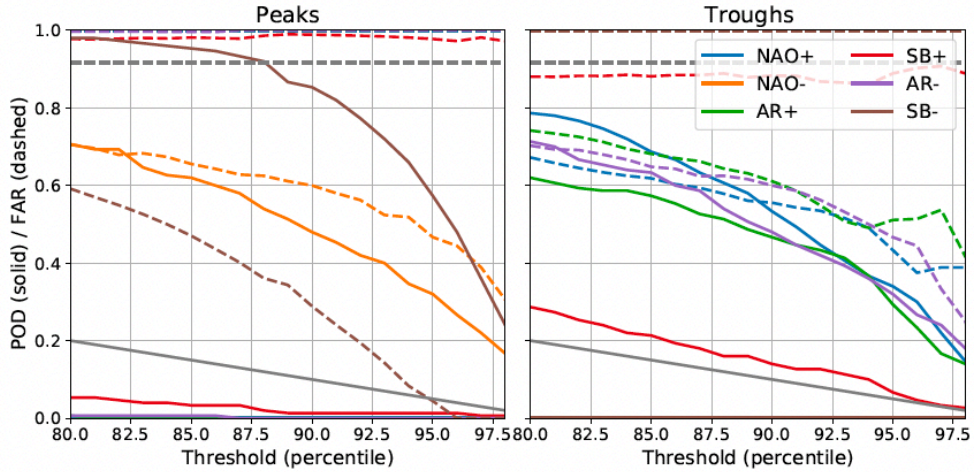
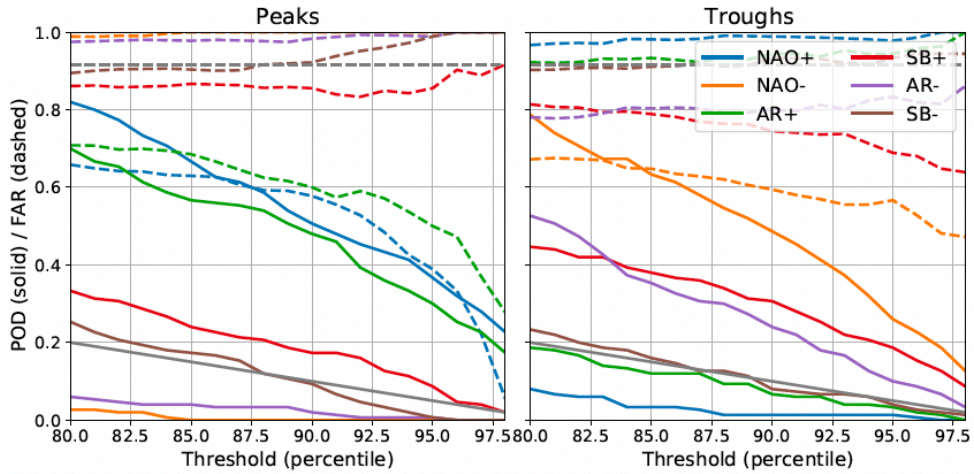


FIG. 10: The interannual variability of the regime frequency for the ensemble Bayesian approach when applied to (random) ensembles of 10 members. In total 50 random ensembles are shown. The solid red and dash-dotted blue lines indicate very strong El Niño and strong La Niña years respectively.

553 Using the sequential Bayesian approach we already find some predictable signal for the NAO+
 554 and SB- regimes, with Bayes factors of 7.6 and 5.1 respectively (Table 1). The Bayes factor for
 555 NAO- is also above 3, but here the p -value is larger reducing the confidence in this being a true
 556 signal. These results are comparable with those found in Falkena et al. (2022), with the regression
 557 coefficients being close to one for NAO+, NAO- and SB-. These regression coefficients around one
 558 indicate the signal in SEAS5 is of similar magnitude to that in ERA-Interim, showing no evidence
 559 of a signal-to-noise paradox for the regime frequencies, in contrast to the NAO-index (Falkena
 560 et al. 2022). Using the ensemble information to update the transition probabilities increases the
 561 predictable signal for NAO+ and SB-, with smaller p -values and higher Bayes factors. Also
 562 the AR- signal is enhanced with a Bayes factor over 3 although the p -value is still relatively
 563 large. The enhancement of the NAO+ signal is comparable to that found using a regularised



(a) El Niño years.



(b) La Niña years.

FIG. 11: The probability of detection (solid) and false alarm ratio (dashed) for a peak or trough in regime frequency in 10-member subsamples of the SEAS5 ensembles occurring in the same year as a very strong El Niño or strong La Niña, as a function of the percentile used for the definition of the peaks and troughs. The colored lines indicate the regime values, and the grey lines the values for peaks and troughs occurring in random years, i.e. no signal.

Regime		NAO+	NAO-	AR+	SB+	AR-	SB-	MLR	NAO-
Sequential Bayes	Reg. Coeff.	1.170	1.094	-0.504	0.258	1.207	1.083	NAO+	-1.369
								SB-	-1.838
	p-value	0.052	0.139	0.592	0.795	0.174	0.082		0.047
	Bayes Fac.	7.579	3.251	1.167	1.037	2.696	5.054		21.108
Ensemble Bayes	Reg. Coeff.	1.066	1.035	-0.435	0.225	1.037	0.785	NAO+	-1.429
								SB-	-1.412
	p-value	0.044	0.133	0.527	0.782	0.136	0.075		0.041
	Bayes Fac.	8.910	3.365	1.240	1.042	3.306	5.487		26.641

TABLE 1: The regression coefficient, p -value and Bayes factor for linear regression of the interannual variability in regime frequency (ERA-Interim onto SEAS5) for all six regimes. In addition, the result of multiple linear regression of the ERA-Interim NAO- frequency against the SEAS5 ensemble mean NAO+ and SB- regime frequencies is shown. Values for both the sequential as well as the ensemble Bayesian approach are shown.

564 clustering approach, whereas the change for SB- is weaker (a Bayes factor of 13.2 compared to
565 5.5, Falkena et al. (2022)). On the other hand, the decrease in Bayes factors for NAO- and AR-
566 using a regularised approach is not found using the ensemble Bayesian method, which shows small
567 increases of the Bayes factors. In Falkena et al. (2022) a significant signal was found using multiple
568 linear regression of ERA-Interim NAO- onto the SEAS5 NAO+ and SB-, which we find here as
569 well with Bayes factors of 21.1 for the sequential method increasing to 26.6 using the ensemble
570 approach. Comparing the two methods, we find that the ensemble Bayesian regime assignment
571 allows to identify more pronounced interannual variability signals for some regimes while still
572 accounting for the signal of the other regimes.

573 6. Conclusion and Discussion

574 A new approach exploiting Bayes Theorem (1) is proposed to obtain a probabilistic regime assign-
575 ment of the atmospheric state on a given day, based on preexisting definitions of the regimes. The
576 approach combines climatological likelihood functions with prior information from the previous
577 day, using climatological estimates of regime persistence, to obtain a Bayesian regime proba-
578 bility. This sequential probabilistic regime assignment allows for smoother transitions between
579 the regimes and indicates whenever data does not clearly belong to one regime. In contrast to
580 previously studied methods that used a regularised k -means clustering algorithm (Falkena et al.
581 2020, 2022) there is no parameter, other than the number of regimes k , that has to be selected.
582 Also, the method can be applied in real time as new data comes in. Applying the approach to

583 six wintertime circulation regimes over the Euro-Atlantic sector yields an increase in persistence,
584 without affecting the average regime frequencies for both SEAS5 and ERA-Interim (Figure 6).
585 In addition, for ERA-Interim the 1-day autocorrelation was found to be higher than that obtained
586 using a regularised k -means approach containing a persistence constraint (Falkena et al. 2020).
587 The Bayesian probabilistic regime assignment can help overcome the need for some of the heuristic
588 devices, such as a “no-regime” category, that are commonly used in circulation regime studies (e.g.
589 Cassou et al. 2005; Grams et al. 2017). The regime probabilities indicate when data cannot be
590 clearly assigned to one regime, whereas the incorporation of prior information ensures persistent
591 regime dynamics. Here, the focus has been on the regime dynamics within the winter season and
592 on interannual timescales, leaving the challenging problem of seasonality of regimes aside (e.g.
593 Breton et al. 2022).

594 A yet more informative prior for the Bayesian approach can be obtained by continuously updating
595 the prior probabilities by taking information from the full SEAS5 ensemble into account. Starting
596 from the assumption of approximate stationarity of the ensemble mean regime frequencies at each
597 day, the regime transition matrix is updated. This update is started from the diagonal of the transition
598 matrix since the persistence dominates the regimes dynamics. The limited availability of data is
599 not sufficient to reliably apply other approaches such as Hidden Markov Models. This updated
600 transition matrix in turn affects the prior probabilities, leading to more pronounced interannual
601 variability for some regimes. When considering the interannual variability, the response to three
602 very strong El Niño events in recent decades clearly stands out (Figure 8). During these three
603 winters SB⁻ and NAO⁻ increase in frequency, while NAO⁺, AR⁺ and AR⁻ decrease. The
604 signals for AR⁺, AR⁻ and SB⁻ are enhanced by the ensemble Bayesian approach compared to
605 the sequential method. The signal during La Niña winters is less pronounced, with the increase in
606 NAO⁺ frequency during 1988-89 standing out most clearly.

607 This response to ENSO in the SEAS5 ensemble can already be identified using only a 10-member
608 ensemble. The increase in SB⁻ occurrence during El Niño years is a particularly strong signal
609 and is found in nearly all 10-member ensembles considered (Figure 10). Also for NAO⁺, NAO⁻,
610 AR⁺ and AR⁻ significant probabilities of detection for peaks or troughs coinciding with El Niño
611 are found. However, here there also is a substantial false alarm ratio indicating that many peaks or
612 troughs in the ensemble occur in non-El Niño years. For La Niña there also is some signal, but not

613 as strong as for El Niño years. These results suggest that one may not need a very large ensemble
614 to identify regime signals in response to ENSO.

615 We also use a linear regression analysis to identify predictable signals in the observations
616 on interannual timescales. Here, as in Falkena et al. (2022), NAO+ and SB- were found to be
617 predictable from the SEAS5 ensemble with regression coefficients around one (Table 1), suggesting
618 no signal-to-noise deficit for these regimes. The ensemble approach leads to an increase in Bayes
619 factor compared to the sequential method for all regimes, with the largest improvement for NAO+.

620 ENSO is certainly part of the reason for the predictable signal found with the regression approach,
621 but it is likely that other processes play a role as well. Previous studies have linked the frequency
622 of Euro-Atlantic circulation regimes to the Madden-Julian Oscillation (e.g. Cassou 2008; Straus
623 et al. 2015; Lee et al. 2019, 2020) and the stratospheric polar vortex (e.g. Charlton-Perez et al.
624 2018; Domeisen et al. 2020), and it would be interesting to see whether the Bayesian approach to
625 regime assignment can aid in better understanding the links between these processes and the regime
626 frequencies. In that respect, the clear improvement in persistence obtained from the sequential
627 method (Figure 5) should be useful for such S2S applications, even if the seasonal averages
628 are not much affected. Information about other climatic processes that are known to affect the
629 regime occurrence can be used to obtain an informative prior for the regime probabilities. For
630 example, knowledge of the states of ENSO or the stratospheric vortex can inform the prior regime
631 probabilities. Such priors can be used for both model ensembles as well as reanalysis datasets and
632 aid in better distinguishing the signal from the noise.

633 The use of the Bayesian regime assignment approach is not limited to atmospheric circulation
634 regimes, but can be applied to any case in which the data can be separated into two or more
635 regimes. For example, one can think of the two phases of the NAO or the jet latitude (Woollings
636 et al. 2010). For the application one needs some information on the regime likelihood function
637 and a way to obtain an informative prior. In most cases the latter will be the most challenging and
638 requires a thorough understanding of the processes involved. For circulation regimes a prior based
639 on climatological transition probabilities, which automatically builds in persistence, was shown to
640 be a suitable and natural choice, and incorporating information from a full ensemble enhanced the
641 interannual signal. Depending on the regime process considered other choices for the prior may
642 be more suitable.

643 *Acknowledgments.* SKJF was supported by the Centre for Doctoral Training in Mathematics of
644 Planet Earth, with funding from the UK Engineering and Physical Sciences Research Council
645 (EPSRC) (grant EP/L016613/1). The research of JdW has been partially funded by Deutsche
646 Forschungsgemeinschaft (DFG) – SFB1294/1, 318763901. We thank the three reviewers for their
647 constructive feedback.

648 *Data availability statement.* ERA-Interim and SEAS5 hindcast data are publicly available at the
649 ECMWF website.

650 **References**

651 Acevedo, W., J. de Wiljes, and S. Reich, 2017: Second-order accurate ensemble transform particle
652 filters. *SIAM Journal on Scientific Computing*, **39** (5), A1834–A1850, [https://doi.org/10.1137/](https://doi.org/10.1137/16M1095184)
653 [16M1095184](https://doi.org/10.1137/16M1095184).

654 Ayarzaguen, B., S. Ineson, N. J. Dunstone, M. P. Baldwin, and A. A. Scaife, 2018: Intraseasonal
655 Effects of El Niño–Southern Oscillation on North Atlantic Climate. *Journal of Climate*, **31** (21),
656 8861–8873, <https://doi.org/10.1175/JCLI-D-18-0097.1>.

657 Baldo, A., and R. Locatelli, 2022: A probabilistic view on modelling weather regimes. *International*
658 *Journal of Climatology*, **n/a** (n/a), <https://doi.org/https://doi.org/10.1002/joc.7942>.

659 Baum, L. E., T. Petrie, G. Soules, and N. Weiss, 1970: A maximization technique occurring in
660 the statistical analysis of probabilistic functions of markov chains. *The annals of mathematical*
661 *statistics*, **41** (1), 164–171.

662 Breton, F., M. Vrac, P. Yiou, P. Vaittinada Ayar, and A. Jézéquel, 2022: Seasonal circulation
663 regimes in the north atlantic: Towards a new seasonality. *International Journal of Climatology*,
664 **42** (11), 5848–5870, <https://doi.org/https://doi.org/10.1002/joc.7565>.

665 Büeler, D., L. Ferranti, L. Magnusson, J. F. Quinting, and C. M. Grams, 2021: Year-round sub-
666 seasonal forecast skill for Atlantic–European weather regimes. *Quarterly Journal of the Royal*
667 *Meteorological Society*, **147** (741), 4283–4309, <https://doi.org/10.1002/qj.4178>.

668 Cassou, C., 2008: Intraseasonal interaction between the Madden-Julian Oscillation and the North
669 Atlantic Oscillation. *Nature*, **455** (7212), 523–527, <https://doi.org/10.1038/nature07286>.

- 670 Cassou, C., T. Laurent, and A. S. Phillips, 2005: Tropical Atlantic Influence on European Heat
671 Waves. *Journal of Climate*, **18 (15)**, 2805–2811, <https://doi.org/10.1175/JCLI3506.1>.
- 672 Charlton-Perez, A. J., L. Ferranti, and R. W. Lee, 2018: The influence of the stratospheric state
673 on North Atlantic weather regimes. *Quarterly Journal of the Royal Meteorological Society*,
674 **144 (713)**, 1140–1151, <https://doi.org/10.1002/qj.3280>.
- 675 Cortesi, N., V. Torralba, L. Lledó, A. Manrique, S. Nube, and G. Reviriego, 2021: Yearly evolution
676 of Euro-Atlantic weather regimes and of their sub-seasonal predictability. *Climate Dynamics*,
677 **56**, 3933–3964, <https://doi.org/10.1007/s00382-021-05679-y>.
- 678 Corti, S., F. Molteni, and T. N. Palmer, 1999: Signature of recent climate change in frequencies of
679 natural atmospheric circulation regimes. *Nature*, **398 (6730)**, 799–802, [https://doi.org/10.1038/](https://doi.org/10.1038/19745)
680 19745.
- 681 Dee, D. P., and Coauthors, 2011: The ERA-Interim reanalysis: Configuration and performance of
682 the data assimilation system. *Quarterly Journal of the Royal Meteorological Society*, **137 (656)**,
683 553–597, <https://doi.org/10.1002/qj.828>.
- 684 Del Moral, P., 1997: Nonlinear filtering: Interacting particle resolution. *Comptes Rendus de*
685 *l'Académie des Sciences-Series I-Mathematics*, **325 (6)**, 653–658.
- 686 Dempster, A. P., N. M. Laird, and D. B. Rubin, 1977: Maximum likelihood from incomplete data
687 via the em algorithm. *Journal of the Royal Statistical Society: Series B (Methodological)*, **39 (1)**,
688 1–22.
- 689 Domeisen, D. I. V., C. M. Grams, and L. Papritz, 2020: The role of North Atlantic-European
690 weather regimes in the surface impact of sudden stratospheric warming events. *Weather and*
691 *Climate Dynamics*, **1**, 373–388, <https://doi.org/10.5194/wcd-1-373-2020>.
- 692 Dorrington, J., K. Strommen, F. Fabiano, and F. Molteni, 2022: Cmp6 models trend toward
693 less persistent european blocking regimes in a warming climate. *Geophysical Research Letters*,
694 **49 (24)**, e2022GL100811.
- 695 Doucet, A., N. De Freitas, N. J. Gordon, and Coauthors, 2001: *Sequential Monte Carlo methods*
696 *in practice*, Vol. 1. Springer.

- 697 Evensen, G., and P. J. van Leeuwen, 2000: An ensemble kalman smoother for nonlinear dynamics.
698 *Mon. Wea. Rev.*, **128** (6), 1852–1867.
- 699 Falkena, S. K. J., J. de Wiljes, A. Weisheimer, and T. G. Shepherd, 2020: Revisiting the Identifica-
700 tion of Wintertime Atmospheric Circulation Regimes in the Euro–Atlantic Sector. *Quarterly Jour-*
701 *nal of the Royal Meteorological Society*, **146** (731), 2801–2814, <https://doi.org/10.1002/qj.3818>,
702 1912.10838.
- 703 Falkena, S. K. J., J. de Wiljes, A. Weisheimer, and T. G. Shepherd, 2022: Detection of inter-
704 annual ensemble forecast signals over the North Atlantic and Europe using atmospheric circu-
705 lation regimes. *Quarterly Journal of the Royal Meteorological Society*, **148** (742), 434–453,
706 <https://doi.org/10.1002/qj.4213>.
- 707 Ferranti, L., S. Corti, and M. Janousek, 2015: Flow-dependent verification of the ECMWF
708 ensemble over the Euro-Atlantic sector. *Quarterly Journal of the Royal Meteorological Society*,
709 **141** (688), 916–924, <https://doi.org/10.1002/qj.2411>.
- 710 Franzke, C. L. E., D. T. Crommelin, A. Fischer, and A. J. Majda, 2008: A hidden Markov model
711 perspective on regimes and metastability in atmospheric flows. *Journal of Climate*, **21** (8),
712 1740–1757, <https://doi.org/10.1175/2007JCLI1751.1>.
- 713 Franzke, C. L. E., T. J. O’Kane, D. P. Monselesan, J. S. Risbey, and I. Horenko, 2015: Systematic
714 attribution of observed Southern Hemisphere circulation. *Nonlinear Processes in Geophysics*,
715 **22**, 513–525, <https://doi.org/10.5194/npg-22-513-2015>.
- 716 Grams, C. M., R. Beerli, S. Pfenninger, I. Staffell, and H. Wernli, 2017: Balancing Europe’s
717 wind-power output through spatial deployment informed by weather regimes. *Nature Climate*
718 *Change*, **7** (8), 557–562, <https://doi.org/10.1038/NCLIMATE3338>.
- 719 Hamilton, J. D., 1989: A New Approach to the Economic Analysis of Nonstationary Time Series
720 and the Business Cycle. *Econometrica*, **57** (2), 357–384.
- 721 Hannachi, A., and A. O’Neill, 2001: Atmospheric multiple equilibria and non-Gaussian behaviour
722 in model simulations. *Quarterly Journal of the Royal Meteorological Society*, **127** (573), 939–
723 958.

- 724 Hannachi, A., D. M. Straus, C. L. E. Franzke, S. Corti, and T. Woollings, 2017: Low-frequency
725 nonlinearity and regime behavior in the Northern Hemisphere extratropical atmosphere. *Reviews*
726 *of Geophysics*, **55** (1), 199–234, <https://doi.org/10.1002/2015RG000509>.
- 727 Horenko, I., 2010: On clustering of non-stationary meteorological time series. *Dynamics of*
728 *Atmospheres and Oceans*, **49** (2-3), 164–187, <https://doi.org/10.1016/j.dynatmoce.2009.04.003>.
- 729 Horenko, I., 2011a: Nonstationarity in Multifactor Models of Discrete Jump Processes, Memory,
730 and Application to Cloud Modeling. *Journal of the Atmospheric Sciences*, **68** (7), 1493–1506,
731 <https://doi.org/10.1175/2011JAS3692.1>.
- 732 Horenko, I., 2011b: On analysis of nonstationary categorical data time series: Dynamical di-
733 mension reduction, model selection, and applications to computational sociology. *Multiscale*
734 *Modeling & Simulation*, **9** (4), 1700–1726.
- 735 Hu, C.-C., and P. J. van Leeuwen, 2021: A particle flow filter for high-dimensional sys-
736 tem applications. *Quarterly Journal of the Royal Meteorological Society*, **147** (737), 2352–
737 2374, <https://doi.org/https://doi.org/10.1002/qj.4028>, <https://rmets.onlinelibrary.wiley.com/doi/pdf/10.1002/qj.4028>.
- 738
- 739 Jain, A. K., 2010: Data clustering: 50 years beyond K-means. *Pattern Recognition Letters*, **31** (8),
740 651–666, <https://doi.org/10.1016/j.patrec.2009.09.011>.
- 741 Johnson, S. J., and Coauthors, 2019: SEAS5: The new ECMWF seasonal forecast system. *Geo-*
742 *scientific Model Development*, **12** (3), 1087–1117, <https://doi.org/10.5194/gmd-12-1087-2019>.
- 743 Kalman, R. E., 1960: A new approach to linear filtering and prediction problems. *Transaction of*
744 *the ASME Journal of Basic Engineering*, 35–45.
- 745 Kantas, N., A. Beskos, and A. Jasra, 2014: Sequential monte carlo methods for high-dimensional
746 inverse problems: A case study for the navier–stokes equations. *SIAM/ASA Journal on Uncer-*
747 *tainty Quantification*, **2** (1), 464–489, <https://doi.org/10.1137/130930364>.
- 748 Kass, R. E., and A. E. Raftery, 1995: Bayes factors. *Journal of the American Statistical Association*,
749 **90** (430), 773–795, <https://doi.org/10.1080/01621459.1995.10476572>.
- 750 Krolzig, H.-M., 1997: *Markov-Switching Vector Autoregressions*. Springer-Verlag.

- 751 Lee, J. C. K., R. W. Lee, S. J. Woolnough, and L. J. Boxall, 2020: The links between the Madden-
752 Julian Oscillation and European weather regimes. *Theoretical and Applied Climatology*, **141**,
753 567–586, <https://doi.org/10.1007/s00704-020-03223-2>.
- 754 Lee, R. W., S. J. Woolnough, A. J. Charlton-Perez, and F. Vitart, 2019: ENSO Modulation of
755 MJO Teleconnections to the North Atlantic and Europe. *Geophysical Research Letters*, **46**,
756 13,535–13,545, <https://doi.org/10.1029/2019GL084683>.
- 757 Majda, A. J., C. L. Franzke, A. Fischer, and D. T. Crommelin, 2006: Distinct metastable at-
758 mospheric regimes despite nearly Gaussian statistics: A paradigm model. *Proceedings of the*
759 *National Academy of Sciences*, **103 (22)**, 8309–8314, <https://doi.org/10.1073/pnas.0602641103>.
- 760 Matsueda, M., and T. N. Palmer, 2018: Estimates of flow-dependent predictability of winter-
761 time Euro-Atlantic weather regimes in medium-range forecasts. *Quarterly Journal of the Royal*
762 *Meteorological Society*, **144 (713)**, 1012–1027, <https://doi.org/10.1002/qj.3265>.
- 763 Michelangeli, P.-A., R. Vautard, and B. Legras, 1995: Weather Regimes: Recurrence and Quasi
764 Stationarity. *Journal of Atmospheric Sciences*, **52 (8)**, 1237–1256.
- 765 Mo, K., and M. Ghil, 1988: Cluster analysis of multiple planetary flow regimes. *Journal of*
766 *Geophysical Research*, **93 (D9)**, 10,927–10,952, <https://doi.org/10.1029/jd093id09p10927>.
- 767 Molteni, F., S. Tibaldi, and T. N. Palmer, 1990: Regimes in the wintertime circulation over northern
768 extratropics. I: Observational Evidence. *Quarterly Journal of the Royal Meteorological Society*,
769 **116**, 31–67.
- 770 O’Kane, T. J., J. S. Risbey, C. Franzke, I. Horenko, and D. P. Monselesan, 2013: Changes
771 in the Metastability of the Midlatitude Southern Hemisphere Circulation and the Utility of
772 Nonstationary Cluster Analysis and Split-Flow Blocking Indices as Diagnostic Tools. *Journal*
773 *of the Atmospheric Sciences*, **70 (3)**, 824–842, <https://doi.org/10.1175/JAS-D-12-028.1>.
- 774 Quinn, C., D. Harries, and T. J. O’Kane, 2021: Dynamical analysis of a reduced model for the North
775 Atlantic Oscillation. *Journal of the Atmospheric Sciences*, **78 (5)**, 1647–1671, <https://doi.org/10.1175/JAS-D-20-0282.1>.
- 776
- 777 Rabiner, L., 1989: A tutorial on hidden markov models and selected applications in speech
778 recognition. *Proceedings of the IEEE*, **77 (2)**, 257–286, <https://doi.org/10.1109/5.18626>.

- 779 Smyth, P., K. Ide, and M. Ghil, 1999: Multiple Regimes in Northern Hemisphere Height Fields
780 via Mixture Model Clustering. *Journal of the Atmospheric Sciences*, **56 (21)**, 3704–3723,
781 [https://doi.org/10.1175/1520-0469\(1999\)056<3704:mrinhh>2.0.co;2](https://doi.org/10.1175/1520-0469(1999)056<3704:mrinhh>2.0.co;2).
- 782 Straus, D. M., S. Corti, and F. Molteni, 2007: Circulation regimes: Chaotic variability versus
783 SST-forced predictability. *Journal of Climate*, **20 (10)**, 2251–2272, [https://doi.org/10.1175/
784 JCLI4070.1](https://doi.org/10.1175/JCLI4070.1).
- 785 Straus, D. M., and F. Molteni, 2004: Circulation Regimes and SST Forcing: Results from Large
786 GCM Ensembles. *Journal of Climate*, **17 (8)**, 1641–1656.
- 787 Straus, D. M., E. Swenson, and C.-L. Lappen, 2015: The MJO Cycle Forcing of the North Atlantic
788 Circulation: Intervention Experiments with the Community Earth System Model. *Journal of the
789 Atmospheric Sciences*, **72 (2)**, 660–681, <https://doi.org/10.1175/jas-d-14-0145.1>.
- 790 Thompson, V., N. J. Dunstone, A. A. Scaife, D. M. Smith, J. M. Slingo, S. Brown, and S. E. Belcher,
791 2017: High risk of unprecedented UK rainfall in the current climate. *Nature Communications*,
792 **8 (107)**, <https://doi.org/10.1038/s41467-017-00275-3>.
- 793 Toniazzo, T., and A. A. Scaife, 2006: The influence of ENSO on winter North Atlantic climate.
794 *Geophysical Research Letters*, **33 (L24704)**, <https://doi.org/10.1029/2006GL027881>.
- 795 Trenberth, K. E., 1997: The definition of el niño. *Bulletin of the American Meteorological Society*,
796 **78 (12)**, 2771 – 2778, [https://doi.org/10.1175/1520-0477\(1997\)078<2771:TDOENO>2.0.CO;2](https://doi.org/10.1175/1520-0477(1997)078<2771:TDOENO>2.0.CO;2).
- 797 van der Wiel, K., H. C. Bloomfield, R. W. Lee, L. P. Stoop, R. Blackport, J. A. Screen, and F. M.
798 Selten, 2019: The influence of weather regimes on European renewable energy production and
799 demand. *Environmental Research Letters*, **14 (094010)**.
- 800 Vautard, R., 1990: Multiple Weather Regimes over the North Atlantic: Analysis of Precursors and
801 Successors. *Monthly Weather Review*, **118**, 2056–2081.
- 802 Vecchi, E., L. Pospíšil, S. Albrecht, T. J. O’Kane, and I. Horenko, 2022: eSPA+: Scalable Entropy-
803 Optimal Machine Learning Classification for Small Data Problems. *Neural Computation*, **34**,
804 1220–1255.

- 805 Vigaud, N., A. W. Robertson, and M. Tippett, 2018: Predictability of Recurrent Weather Regimes
806 over North America during Winter from Submonthly Reforecasts. *Monthly Weather Review*,
807 **146**, 2559–2577, <https://doi.org/10.1175/MWR-D-18-0058.1>.
- 808 Viterbi, A., 1967: Error bounds for convolutional codes and an asymptotically optimum decoding
809 algorithm. *IEEE transactions on Information Theory*, **13 (2)**, 260–269.
- 810 Wagenmakers, E.-J., 2007: A practical solution to the pervasive problems of p values. *Psychonomic*
811 *Bulletin & Review*, **14 (5)**, 779–804.
- 812 Woollings, T., A. Hannachi, and B. Hoskins, 2010: Variability of the North Atlantic eddy-
813 driven jet stream. *Quarterly Journal of the Royal Meteorological Society*, **136 (649)**, 856–868,
814 <https://doi.org/10.1002/qj.625>.